Anoxia decreases the magnitude of the carbon, nitrogen, and phosphorus sink in freshwaters

Cayelan C. Carey[1]*, Paul C. Hanson[2], R. Quinn Thomas[1,3], Alexandra B. Gerling[1], Alexandria G. Hounshell[1], Abigail S. L. Lewis[1], Mary E. Lofton[1], Ryan P. McClure[1], Heather L. Wander[1], Whitney M. Woelmer[1], B. R. Niederlehner[1], Madeline E. Schreiber[4]

[1]Department of Biological Sciences, Virginia Tech, Blacksburg, Virginia, USA 24061.

[2]Center for Limnology, University of Wisconsin-Madison, Madison, Wisconsin, USA 53706.

[3]Department of Forest Resources and Environmental Conservation, Virginia Tech, Blacksburg, Virginia, USA 24061.

[4]Department of Geosciences, Virginia Tech, Blacksburg, Virginia, USA 24061.

*Corresponding author. Email: cayelan@vt.edu; Phone: +1-540-231-8938

ORCID iDs:

Carey: 0000-0001-8835-4476

Hanson: 0000-0001-8533-6061

Thomas: 0000-0003-1282-7825

Gerling: 0000-0001-5280-6709

Hounshell: 0000-0003-1616-9399

Lewis: 0000-0001-9933-4542

Lofton: 0000-0003-3270-1330

McClure: 0000-0001-6370-3852

Wander: 0000-0002-3762-6045

Woelmer: 0000-0001-5147-3877

Niederlehner: 0000-0002-6933-336X

Schreiber: 0000-0002-1858-7730

Accepted as a **Primary Research Article** at *Global Change Biology*

Running title: Anoxia disrupts freshwater C, N, and P cycles

Data Availability Statement: All data and code are available in the Environmental Data Initiative repository (Carey et al. 2019, Carey et al. 2020, Carey et al. 2021a, Carey et al. 2021b, Carey et al. 2021c, Carey et al. 2021d, Carey et al. 2022a) and Zenodo repository (Carey et al. 2022b).

Abstract

Oxygen availability is decreasing in many lakes and reservoirs worldwide, raising the urgency for understanding how anoxia (low oxygen) affects coupled biogeochemical cycling, which has major implications for water quality, food webs, and ecosystem functioning. Although the increasing magnitude and prevalence of anoxia has been documented in freshwaters globally, the challenges of disentangling oxygen and temperature responses have hindered assessment of the effects of anoxia on carbon, nitrogen, and phosphorus concentrations, stoichiometry (chemical ratios), and retention in freshwaters. The consequences of anoxia are likely severe and may be irreversible, necessitating ecosystem-scale experimental investigation of decreasing freshwater oxygen availability. To address this gap, we devised and conducted REDOX (the Reservoir Ecosystem Dynamic Oxygenation eXperiment), an unprecedented, seven-year

experiment in which we manipulated and modeled bottom-water (hypolimnetic) oxygen availability at the whole-ecosystem scale in a eutrophic reservoir. Seven years of data reveal that anoxia significantly increased hypolimnetic carbon, nitrogen, and phosphorus concentrations and altered elemental stoichiometry by factors of 2-5× relative to oxic periods. Importantly, prolonged summer anoxia increased nitrogen export from the reservoir by six-fold and changed the reservoir from a net sink to a net source of phosphorus and organic carbon downstream. While low oxygen in freshwaters is thought of as a response to land use and climate change, results from REDOX demonstrate that low oxygen can also be a *driver* of major changes to freshwater biogeochemical cycling, which may serve as an intensifying feedback that increases anoxia in downstream waterbodies. Consequently, as climate and land use change continue to increase the prevalence of anoxia in lakes and reservoirs globally, it is likely that anoxia will have major effects on freshwater carbon, nitrogen, and phosphorus budgets as well as water quality and ecosystem functioning.

Keywords: Biogeochemistry, Ecosystem modeling, Hypoxia, Nutrient retention, Oxygen, REDOX, Reservoir, Stoichiometry, Water quality, Whole-ecosystem experiment

Introduction

Oxygen concentrations in lakes and reservoirs around the world are decreasing, which has the potential to substantially alter freshwater ecosystem functioning and water quality. As a result of climate and land use change, low oxygen availability (anoxia) is becoming more common in the hypolimnion, or bottom waters, of many lakes and reservoirs (Jenny et al. 2016a, Jane et al. 2021, Woolway et al. 2021). An increase in both the occurrence and duration of

hypolimnetic anoxia in freshwaters is likely to substantially alter the cycles of carbon (C), nitrogen (N), and phosphorus (P), three fundamental elements that determine freshwater food web structure, water quality, and ecosystem functioning (Sterner and Elser 2002, Kortelainen et al. 2013). In particular, anoxia could disrupt the critical role of freshwater ecosystems as C, N, and P sinks in global biogeochemical cycles. Freshwaters retain 72% of the organic C, 56% of the total N, and 56% of the total P exported from land via sediment burial or release to the atmosphere, preventing these elements from being transported to downstream freshwater ecosystems or the oceans (Maranger et al. 2018). Altogether, the consequences of anoxia for C, N, and P concentrations, stoichiometry (chemical ratios), and retention in freshwaters are likely severe and may be irreversible (Nürnberg 1988, Søndergaard et al. 2003, Brothers et al. 2014, North et al. 2014), necessitating ecosystem-scale investigation of how hypolimnetic anoxia affects freshwaters.

Biogeochemical cycles of dissolved and total C, N, and P will likely respond differently to hypolimnetic anoxia (Fig. 1). In the bottom waters of lakes and reservoirs, we expect dissolved organic C (DOC) concentrations to be higher in anoxic than oxic conditions, as DOC is mineralized much more efficiently by oxygen than by alternate terminal electron acceptors (Walker and Snodgrass 1986, Beutel 2003). Moreover, anoxia has been shown to stimulate the release of DOC from sediments to the water column (Fig. 1; Brothers et al. 2014, Peter et al. 2017), as well as increase hypolimnetic methane concentrations and subsequent greenhouse gas emissions (Bartosiewicz et al. 2019, Vachon et al. 2019, Hounshell et al. 2021). DOC generally dominates the total OC (TOC) pool in lakes (Toming et al. 2020), thus we would expect TOC to exhibit similar responses as DOC to anoxia. For hypolimnetic dissolved inorganic nitrogen (DIN), ammonium (NH_4^+) concentrations would be expected to be higher in anoxic conditions

due to ammonification and release from sediments (Fig. 1; Rysgaard et al. 1994, Beutel et al. 2006). In contrast, nitrate (NO_3^-) would be lower in anoxic than oxic conditions, as denitrification decreases NO_3^- in the absence of oxygen while nitrification increases NO_3^- in the presence of oxygen (Fig. 1; Sharma and Ahlert 1977, Downes 1987). Total nitrogen (TN) in the hypolimnion could either increase or decrease in anoxic conditions, depending on the balance of NH_4^+ vs. NO_3^- within the DIN pool, as the inorganic fraction of hypolimnetic dissolved N is generally greater than the organic fraction (Kim et al. 2006). For hypolimnetic phosphorus (P), we would expect that dissolved reactive phosphorus (DRP) concentrations would be higher in anoxic conditions as DRP is released into the water column during iron reduction and particulate organic matter mineralization (Fig. 1; Mortimer 1971, Boström et al. 1988, Nürnberg 1988, Rydin 2000). Total P (TP) concentrations would likely exhibit a similar but more muted response to anoxia than DRP, as DRP is usually a small fraction of the TP pool (Wetzel 2001).

While these different C, N, and P processes have been well-studied individually, there have been no studies on the net effect of anoxia on all of these cycles operating concurrently at the ecosystem scale, likely due to the challenges of disentangling complex coupled biogeochemical cycling with observational field studies or laboratory experiments. Explicitly considering interconnected elemental cycles and their stoichiometry (following Sterner and Elser 2002) is essential to understanding the effects of anoxia on ecosystem functioning.

Increases in hypolimnetic anoxia have substantial implications for the fate of C, N, and P in freshwater ecosystems. There are two primary fates for C, N, and P entering into a waterbody: 1) retention, by either remaining in the water column, burial in the sediments, or emission to the atmosphere (for C and N only); or 2) export downstream (following the ecosystem retention definition used by Dillon and Molot 1997, Harrison et al. 2009, Powers et al. 2015, Maranger et

al. 2018, and many others). Anoxia may decrease the ability of lakes and reservoirs to retain NH_4^+ and DRP by reducing their burial in sediments (Rysgaard et al. 1994, North et al. 2014, Powers et al. 2015), thereby increasing their downstream export. Conversely, anoxia could increase the retention of NO_3^- by increasing its emission to the atmosphere via denitrification, thereby decreasing its downstream export (Fig. 1; Beaulieu et al. 2014). For C, the ecosystem-scale effects of anoxia are likely complex. The TOC pool includes dissolved and particulate fractions of OC that may respond to oxygen differently and are mediated by ambient environmental conditions, such as external loading, temperature, nutrients, and light (Hanson et al. 2015). For example, anoxia could increase the retention of particulate OC (POC) by decreasing its mineralization, thereby potentially increasing its burial in sediments (Walker and Snodgrass 1986, Beutel 2003). Simultaneously, anoxia could decrease the retention of DOC by stimulating fluxes of DOC from the sediments into the water column (e.g., by reductive dissolution of iron-bound DOC complexes; Skoog and Arias-Esquivel 2009), thereby potentially decreasing burial in sediments (Brothers et al. 2014, Peter et al. 2017), and increasing DOC export downstream. Consequently, quantifying the effect of anoxia on C, N, and P retention vs. downstream export (and thus determining if a waterbody is a sink or source of C, N, and P downstream) is needed to improve our understanding of the changing role of lakes and reservoirs in global biogeochemical cycles.

In particular, human-made reservoirs, which retain substantially more inflowing C, N, and P per unit area than naturally formed lakes globally via either sediment burial or emissions to the atmosphere (Harrison et al. 2009, Powers et al. 2016, Maranger et al. 2018), may be very sensitive to the effects of hypolimnetic anoxia. Despite only covering 6-11% of the global lentic surface (Downing et al. 2006, Lehner et al. 2011, Verpoorter et al. 2014), reservoirs alone are

139 estimated to account for ~40% of total annual global OC burial (Mendonça et al. 2017) and 26%
140 of total annual global P burial (Maranger et al. 2018). Moreover, reservoirs globally emit 6.5 Tg
141 N yr^{-1} to the atmosphere, primarily via denitrification (Harrison et al. 2009, Beusen et al. 2016).
142 In an analysis of ~1000 lakes and reservoirs sampled once across the U.S., reservoirs were found
143 to have lower organic C:P and N:P ratios than naturally formed lakes, which was attributed in
144 part to a greater incidence of hypolimnetic anoxia in reservoirs than naturally formed lakes
145 (Maranger et al. 2018). However, that study lacked accompanying oxygen data to examine how
146 C, N, and P varied across a gradient of oxygen availability. Moreover, the amalgamation of data
147 from waterbodies with different climate and catchment land use makes it challenging to quantify
148 how changing oxygen alters water column C, N, and P concentrations, stoichiometry, and export.
149 We need new approaches that embrace the dynamic nature of reservoirs over time and allow us
150 to disentangle the effects of hypolimnetic anoxia on these waterbodies, especially as their
151 construction is increasing globally (Zarfl et al. 2015).
152 To mechanistically quantify the effects of anoxia on C, N, and P cycling, we devised and
153 conducted REDOX (the Reservoir Ecosystem Dynamic Oxygenation eXperiment), an
154 unprecedented, seven-year study that integrated a long-term hypolimnetic oxygenation
155 manipulation with ecosystem modeling in a eutrophic reservoir. Coupled whole-ecosystem
156 manipulations and ecosystem modeling provide a powerful approach for both quantifying the
157 effects of hypolimnetic anoxia on C, N, and P cycling and testing the mechanisms underlying
158 continental-scale patterns derived from thousands of waterbodies (e.g., Helton et al. 2015,
159 Maranger et al. 2018). Foundational work based on sediment core incubations in the laboratory
160 and small chambers placed *in situ* on the sediments of lakes and reservoirs (e.g., Frindte et al.
161 2015, Lau et al. 2016) have yet to be tested at the ecosystem scale, which is needed to overcome

the limitations of small volumes of water and mesocosm fouling. Studies that manipulate an entire ecosystem are able to disentangle the effects of oxygen availability from other environmental drivers, such as water temperature and biological activity, on C, N, and P cycling (Cole 2013). However, it is logistically challenging to replicate these intensive experiments under different meteorological and environmental conditions over time to assess robustness and repeatability of ecosystem responses. Consequently, data from whole-ecosystem manipulations can be used to calibrate ecosystem models (following Medlyn et al. 2015) that can simulate complex ecosystem responses under a range of oxygen scenarios and weather conditions over multiple years, thereby overcoming the constraints of separate empirical and model investigations.

The purpose of REDOX was to study ecosystem-scale functioning under contrasting oxygen conditions over multiple years in the same reservoir. First, we intensively monitored dissolved oxygen and total and dissolved C, N, and P chemistry, as well as a suite of accompanying water quality variables, in the reservoir during the seven-year field manipulation. Second, we used the empirical data to calibrate a coupled hydrodynamic-ecosystem model, which was used to quantify the effects of varying oxygen conditions over the seven years. To further investigate changes in reservoir C, N, and P cycling due to anoxia, we used the calibrated model to test hypolimnetic oxygen scenarios under a range of seasonal and meteorological conditions. We focused on two contrasting model scenarios: one in which there was oxygenation throughout the stratified summer periods in all seven years, resulting in continuous oxic conditions, and one in which there was no oxygenation, resulting in hypolimnetic anoxia every summer. We used the model output to address the following questions: 1) How does hypolimnetic oxygen availability affect total and dissolved C, N, and P concentrations and

185 stoichiometry?, and 2) How does hypolimnetic anoxia affect reservoir retention and downstream
186 export of C, N, and P?
187
188 **Materials and Methods**
189 *Site description*
190 We studied the effect of changing oxygen conditions on C, N, and P dynamics in Falling
191 Creek Reservoir (FCR), a small eutrophic reservoir located in Vinton, Virginia, USA
192 (37.303479,-79.837371; Fig. 2). FCR has a maximum depth of 9.3 m and surface area of 0.119
193 km^2 and is a drinking water source operated by the Western Virginia Water Authority (WVWA;
194 Gerling et al. 2014). FCR's watershed was farmland at the time of reservoir construction in 1898
195 and is almost completely deciduous forest today following agricultural abandonment in the
196 1930s (Gerling et al. 2016). The reservoir has never been dredged (Gerling et al. 2016), and had
197 a mean hydraulic residence time of 281 days (±12 days, 1 S.E.) during our study. FCR has
198 hypolimnetic outtake valves from which water can be withdrawn for treatment.
199
200 *Whole-ecosystem manipulations*
201 We manipulated hypolimnetic oxygen availability in FCR using an engineered
202 hypolimnetic oxygenation system (HOx) deployed by the WVWA in 2012, which allowed us to
203 generate contrasting summer oxic and anoxic conditions (Gerling et al. 2014). The HOx system
204 withdraws hypolimnetic water from 8 m depth, injects dissolved oxygen into the water at super-
205 saturated concentrations onshore, and returns the oxygenated water back to the hypolimnion at 8
206 m without altering thermal stratification or water temperature (Gerling et al. 2014).

During the summers of 2013-2019, the HOx system was operated at variable oxygen addition levels and durations in collaboration with the WVWA (Carey et al. 2022a). Some summers experienced intermittent 4-week periods of oxygenation (2013, 2014); some summers had near-continuous oxygenation (2015, 2016, 2017), one summer had approximately half oxygenation (2018), and one summer experienced intermittent 2-week periods of oxygenation (2019; Carey et al. 2022a). These wide-ranging oxygenation conditions, which occurred because the reservoir was an actively managed drinking water source, provided an ideal dataset for calibrating the biogeochemical rates in the ecosystem model to variable hypolimnetic oxygen conditions, as described below.

Monitoring data

FCR's physics, chemistry, and biology were intensively monitored throughout the REDOX manipulations (see Supporting Information Text 1 for detailed field sampling methods). On every sampling day, depth profiles of water temperature and dissolved oxygen were collected at the deepest site of the reservoir, near the dam (Carey et al. 2021b). We collected water samples for total and dissolved N, P, and organic C (hereafter, C) analyses from the reservoir's water treatment extraction depths (0.1, 1.6, 2.8, 3.8, 5.0, 6.2, 8.0, and 9.0 m) using a Van Dorn sampler. Water was filtered through glass-fiber 0.7-micron filters into acid-washed bottles and immediately frozen until analysis for dissolved C, N, and P samples (Carey et al. 2021c). Unfiltered water was frozen in separate acid-washed bottles for total samples (Carey et al. 2021c). We focused our sampling and analysis on organic C, rather than inorganic C, because of the important role of reservoirs in burying this pool in the global C cycle (Mendonça et al. 2017), and because previous work indicates that most terrestrial dissolved inorganic C loads are rapidly

emitted to the atmosphere (McDonald et al. 2013).

We used standard methods for biogeochemical analyses (see Supporting Information Text 2 for detailed laboratory methods). We used flow injection analysis to determine concentrations of N and P colorimetrically (APHA 2017), with an alkaline persulfate digestion for TN and TP fractions. DOC and TOC were determined by either heated persulfate digestion or high-temperature combustion followed by infrared absorbance (APHA 2017; see Table S1). All field and laboratory data are available with detailed metadata in the Environmental Data Initiative (EDI) repository (Carey et al. 2019, Carey et al. 2020, Carey et al. 2021a, Carey et al. 2021b, Carey et al. 2021c, Carey et al. 2021d).

Model description and driver data

We used the empirical data to calibrate and validate the General Lake Model coupled to Aquatic EcoDynamics modules (GLM-AED, v.3.2.0a3) configured for FCR (see Supporting Information Text 3 for detailed modeling methods). GLM-AED is an open-source, 1-D numerical simulation model that is widely used in the freshwater research community to model lakes and reservoirs (e.g., Bruce et al. 2018, Hipsey et al. 2019, Farrell et al. 2020, Ward et al. 2020, Hipsey 2022). GLM-AED requires meteorological, inflow, and outflow driver data and simulates water balance and thermal layers using a Lagrangian strategy (Hipsey et al. 2019, Hipsey 2022). GLM-AED has a flexible structure in which modules representing different ecosystem components can be turned on or off to recreate varying levels of ecosystem complexity; our configuration for FCR included modules for oxygen, C, silica (Si), N, P, organic matter, and phytoplankton (Carey et al. 2022a, Carey et al. 2022b).

GLM-AED simulates the dominant processes controlling freshwater oxygen and C, N, and P cycling (see Supporting Information Text 3; Hipsey 2022). Biogeochemical processes (e.g., sediment fluxes, mineralization) were modeled as a function of both oxygen following Michaelis-Menten dynamics and temperature following Arrhenius coefficients (Farrell et al. 2020). Consequently, processes that are favored in anoxic conditions (e.g., sediment fluxes of DOC, NH_4^+, and DRP into the hypolimnion) were still simulated in oxic conditions, but at much lower rates.

The ecosystem model provided important insight on the effects of anoxia that would have been impossible to obtain from the field manipulation alone. First, while we do report on the biogeochemical responses to the field manipulation to provide complementary data to the model output, ecosystems rarely experience such rapid shifting of redox conditions at sub-seasonal scales, as were created by abrupt additions of oxygen via the HOx system. Thus, to understand how our FCR results applied to other waterbodies, we used the seven-year field manipulation as a proxy to contrast the consequences of seasonally oxic vs. anoxic hypolimnia for biogeochemical cycling in an ecosystem model. These highly contrasting scenarios were achieved in the model by manipulating hypolimnetic oxygen injection (described below). Second, to determine the cumulative fate of C, N, and P over an entire summer in response to oxygen dynamics, it is important to track these elements at a high temporal resolution. Because our field data were collected weekly to monthly, we used numerical modeling of hydrodynamics and ecosystem processes to capture daily dynamics. Third, the field manipulation included a variable oxygenation schedule which occurred against a backdrop of changing meteorology and hydrology. Consequently, the model enabled us to isolate the effects of oxygen availability on

the reservoir's biogeochemistry and evaluate the robustness of ecosystem responses across varying environmental conditions.

Model configuration and calibration

All GLM-AED model configuration files, parameters, and driver data for FCR are available in the EDI repository (Carey et al. 2022a). GLM-AED driver data included hourly meteorological data from NASA's North American Land Data Assimilation System (NLDAS-2; Xia et al. 2012), stream inflow data, and outflow data. We developed stream inflow driver datasets – which consisted of daily discharge, water temperature, and chemistry – for the two primary streams entering FCR from observational data (Supporting Information Text 3). To simulate the HOx system in the model, we added a submerged inflow that injected oxygenated water into the reservoir at 8 m, the same depth as in the reservoir. As the reservoir was managed to keep constant water level, outflow volume was set to equal inflow volume; the physical and chemical properties of the outflow were determined by the state of the modeled reservoir (Supporting Information Text 3).

We ran the model from 15 May 2013 to 31 December 2019, divided into calibration (15 May 2013 - 31 December 2018) and validation (1 January 2019 - 31 December 2019) periods for model verification. GLM-AED was run on an hourly time step throughout the total simulation period (Carey et al. 2022a).

We calibrated GLM-AED to observed conditions (Supporting Information Text 3). First, we conducted a global sensitivity analysis to identify the most important parameters for simulating water temperature, dissolved oxygen, NH_4^+, NO_3^-, DRP, and DOC following Morris (1991). Second, we calibrated the identified sensitive parameters (Table S2) using the covariance

297 matrix adaptation evolution strategy for automated numerical optimization (Hansen 2016) to
298 minimize root mean square error (RMSE) between observations and model output for all
299 sampling depths in the water column.
300 We calculated multiple goodness-of-fit metrics to assess the model's performance during
301 the calibration period, validation period, and total simulation period, including RMSE, the
302 coefficient of determination (R^2), percent bias, and normalized mean absolute error (NMAE)
303 (e.g., Kara et al. 2012, Ward et al. 2020, Ladwig et al. 2021). We calculated these goodness-of-
304 fit metrics following the most common approaches used in 328 recent freshwater modeling
305 studies (reviewed by Soares and Calijuri 2021; described in Supporting Information Text 3).
306
307 *Model scenarios*
308 Following model calibration, we examined the effects of two different oxygen scenarios
309 on FCR's biogeochemistry using the GLM-AED model: 1) an "oxic" scenario in which the
310 model was forced with a high level of oxygenation to keep the hypolimnion oxic throughout
311 summer thermal stratification (May 15 - Oct 15) during 2013-2019; and 2) an "anoxic" scenario
312 in which zero oxygen was added to the hypolimnion, so hypolimnetic anoxia quickly set up after
313 the onset of thermal stratification each summer. All other driver data (meteorology, stream
314 inflows, outflow) were held constant.
315
316 *Statistical analysis*
317 We used several approaches to answer the two research questions. For Q1, we first
318 compared observed data from the oxygenated vs. non-oxygenated periods of our field
319 manipulation to determine if oxygenation had an effect on empirical total and dissolved C, N,

and P concentrations. We pooled all hypolimnetic C, N, and P samples from the two summers with the least oxygenation (July 15 - October 1 in 2018, 2019) when the HOx was deactivated and compared them with concentrations measured during the two summers with the most continuous oxygenation (July 15 - October 1 in 2016, 2017) when the HOx was activated (Supporting Information Text 4). We also used the FCR field data to validate the model's ability to simulate the field manipulation. Second, because our goal was to compare completely oxic vs. completely anoxic summers and every summer had at least some oxygenation during the seven-year field manipulation, we focused our subsequent analyses on the anoxic vs. oxic model scenario output, which provided complementary data to the non-oxygenated vs. oxygenated empirical data. Focusing on the model output for this analysis also enabled us to overcome the limitations of comparing years with different numbers of sampling observations, as the model calculated daily C, N, and P concentrations and rates.

We compared hypolimnetic C, N, and P concentrations and rates between the oxic and anoxic model scenarios during 15 July - 1 October among years, the interval within the summer thermally stratified period when the reservoir consistently exhibited hypolimnetic anoxia in non-oxygenated conditions. We calculated the median hypolimnetic dissolved and total concentrations of C, N, and P during this period for each of the seven years (2013 - 2019), and compared the median summer anoxic and oxic concentrations and their ratios using paired t-tests, as there was no temporal autocorrelation among median summer values (Supporting Information Text 5). We also examined summer rates of all processes controlling increases and decreases in hypolimnetic C, N, and P to determine their relative importance and sensitivity to oxygen.

342 To examine how the uncertainty of our model outputs was affected by the model
343 parameterization, we conducted an additional sensitivity analysis in which we doubled and
344 halved the calibrated values of highly sensitive parameters for DOC, NH_4^+, NO_3^-, and DRP using
345 a one-step-at-a-time (OAT) approach (following Brett et al. 2016). We then re-calculated the
346 summer hypolimnetic concentrations of DOC, NH_4^+, NO_3^-, and DRP in the anoxic and oxic
347 model scenarios for each variable and compared anoxic and oxic concentrations with paired t-
348 tests, as described above (Supporting Information Text 3, Fig. S1).
349 For Q2, we estimated C, N, and P downstream export as a percent of inputs into the
350 reservoir each summer (Powers et al. 2015, Farrell et al. 2020). Downstream export was
351 calculated as:
352 $Flux = 100\% \times ((\Sigma Outputs - \Sigma Inputs)/\Sigma Inputs)$ (eqn. 1)
353 where Outputs and Inputs represent the daily mass of C, N, or P leaving and entering the
354 reservoir, respectively, during 15 July - 1 October each year. Fluxes were calculated for both
355 dissolved and total fractions of C, N, and P. Inputs were calculated by multiplying the individual
356 stream daily inflow concentrations with their daily inflow volumes and then summing across the
357 two streams. Outputs were calculated by multiplying the outflow water volume (leaving the
358 reservoir and going downstream) by hypolimnetic concentrations. A water budget calculated for
359 the reservoir in 2014 - 2015 (Munger et al. 2019) supplemented by monitoring data in this study
360 indicates that the two inflow streams represented approximately 97% of the reservoir's water
361 inputs (Supporting Information Text 1), motivating our focus on those inputs.
362 Inputs and Outputs were summed across the 15 July - 1 October period to calculate C, N,
363 and P fluxes. Flux values of 0 indicated that the reservoir inputs balanced outputs; flux values <0
364 indicated that the reservoir was a net sink of C, N, or P; and flux values >0 indicated that the

reservoir was a net source of C, N, or P downstream. We compared summer retention (i.e., flux values) in the anoxic and oxic scenarios with paired t-tests (Supporting Information Text 5).

To ease comparison among C, N, and P concentrations and ratios, all analyses were conducted in molar units. All analyses were conducted in R v.3.6.3 (R Core Team 2020) and all code to reproduce these analyses is available in the Zenodo repository (Carey et al. 2022b).

Results

Our integrated whole-ecosystem REDOX field manipulation and modeling demonstrates that hypolimnetic anoxia significantly alters water column C, N, and P concentrations and stoichiometry. Importantly, our study also shows that prolonged hypolimnetic anoxia in the summer decreases the ability of a reservoir to retain C, N, and P, substantially increasing the downstream export of these elements.

Observational data from whole-ecosystem manipulations

Injection of oxygen into the bottom waters of Falling Creek Reservoir (FCR) over seven years increased the reservoir's observed hypolimnetic oxygen, resulting in substantial changes in total and dissolved C, N, and P concentrations (Fig. 3, Fig. S2). Due to the nature of our oxygenation manipulation, some years experienced low levels of oxygenation (i.e., the HOx was off for prolonged periods throughout the summer), while others experienced high levels of oxygenation during the stratified period (Fig. 3b). Oxygenation resulted in substantially higher hypolimnetic oxygen concentrations without altering water temperature and thermal stratification in the reservoir (Fig. 3a,b). In 2019, oxygenation did not increase hypolimnetic oxygen

concentrations to the same extent as preceding summers, likely because the HOx was only operated for intermittent 2-week periods (vs. 4-week or longer periods in all other years).

The median observed hypolimnetic DOC, NH_4^+, and DRP concentrations were 2.0, 6.9, and 1.3× higher in the summers with the least oxygenation (2018, 2019) than in the summers with the highest oxygenation (2016, 2017; Fig. 3c,e,h; Fig. S2), respectively. Following the patterns exhibited by the dissolved fractions, median observed hypolimnetic TN and TP concentrations were both 2.4× higher in the low vs. high oxygenation summers (Fig. 3d,g; Fig. S2). Conversely, median observed hypolimnetic NO_3^- concentrations were 5× lower in summers with low oxygenation than summers with high oxygenation (Fig. 3f, Fig. S2). Because our goal was to compare completely oxic vs. completely anoxic summer conditions and every summer had at least some oxygenation during the seven-year field manipulation at varying levels of oxygen injection, subsequent analyses focused on the anoxic vs. oxic model scenario output, described below.

Model performance

The field manipulation data were used to calibrate the ecosystem model, which generally reproduced observed water temperature, oxygen, dissolved and total C, N, and P concentrations, and stoichiometry (Table 1, Fig. 3, Fig. S3, Fig. S4). Similar to field observations, the simulation of oxygen injection in the model did not substantively alter modeled water temperature or thermocline depth (Table 1, Fig. 3a).

Model performance of most state variables in our study (Table 1) exceeded the median goodness-of-fit metrics for recent freshwater modeling studies reported by Soares and Calijuri (2021). For example, our water temperature R^2 was 0.95 for the full seven-year simulation period

(vs. 0.94 in Soares and Calijuri 2021), our dissolved oxygen R^2 was 0.72 (vs. 0.61), our TN was 0.71 (vs. 0.61), and our NH_4^+ R^2 was 0.77 (vs. 0.35). No DOC data were reported by Soares and Calijuri (2021), but our R^2 values ranged from 0.30-0.52 for the full simulation, calibration, and validation periods. Phosphorus had less good fit, but was still reasonable: our TP R^2 was 0.25 for the full seven-year simulation period (slightly lower than the 0.30 reported by Soares and Calijuri 2021), but the validation period's R^2 for TP was much higher, at 0.85. Similarly, our DRP R^2 was 0.10 for the full seven-year period (vs. 0.32) but the six-year calibration period had better performance, at an R^2 of 0.24. NO_3^- had an R^2 of 0.27 for the full seven-year modeling period and R^2 of 0.33 for the six-year calibration period, which was lower than the 0.61 reported by Soares and Calijuri (2021).

Much of the variation in DRP and NO_3^- observations was within the analytical limits of quantitation (Fig. 3f,h). Consequently, while the model generally captured seasonal patterns of DRP and NO_3^-, it was simply not possible to reproduce short-term fluctuations in observations below method detection limits. NO_3^- concentrations in particular were extremely low in both field observations and model output (Fig. 3f). Throughout the study, NO_3^- was a very minor fraction of TN, representing a median of 0.5% (±0.9%, 1 S.D.) of TN at all depths in the field data and a median of 0.8% (±0.9%) of TN in the baseline simulation. Subsequently, a lower fit of NO_3^- did not affect the model performance of TN, as evident by its goodness-of-fit metrics (Table 1).

How does hypolimnetic oxygen availability affect total and dissolved C, N, and P concentrations and stoichiometry?

Model scenarios show that hypolimnetic anoxia significantly affected all three focal

elemental cycles, but that N was the most sensitive (Fig. 4, Fig. 5; see Table S3 for statistics). Summer TN molar concentrations in the reservoir were on average 3.0× higher in anoxic than oxic conditions, relative to a 1.1× increase of TOC and 1.6× increase of TP (Fig. 5a,c,g). The dissolved fractions accounted for most of the changes in total C, N, and P: following the field data, modeled summer hypolimnetic DOC, NH_4^+, and DRP concentrations in FCR were on average 1.1, 5.8, and 3.1× higher, respectively, during anoxic conditions than in oxic conditions (Fig. 5b,e,h). Conversely, hypolimnetic NO_3^- was much lower in anoxic conditions (usually at or just above 0 mmol m^{-3}) than oxic conditions, but DIN exhibited an overall increase because of the dominance of NH_4^+ over NO_3^- in the dissolved inorganic N pool (Fig. 5d,f). The statistical significance and overall magnitude of differences in concentrations between the anoxic and oxic scenarios were consistent even when focal parameters governing DOC, NH_4^+, NO_3^-, and DRP were doubled or halved in the parameter sensitivity analysis (Fig. S1).

The elemental stoichiometry in FCR exhibited rapid and large ecosystem-scale changes after the onset of anoxia each summer. While total and dissolved fractions of C, N (except NO_3^-), and P significantly increased with anoxia (Fig. 4, Fig. 5), the different fractions had varying sensitivities to changing oxygen, resulting in significant changes in C, N, and P ratios (Fig. 6, Table S4). Hypolimnetic TN:TP and DIN:DRP were significantly higher (both by 1.9×, on average) in anoxic conditions than oxic conditions (Fig. 6g,h). Because modeled hypolimnetic NO_3^- concentrations were at or near zero during anoxic conditions (Fig. 5f), DOC:NO_3^- could not be consistently calculated (Fig. 6e). In contrast, TOC:TN, TOC:TP, DOC:DIN, DOC:NH_4^+, and DOC:DRP were significantly higher (on average, by 2.7×, 0.7×, 4.7×, 5.0×, and 2.7×, respectively) in oxic conditions than anoxic conditions (Fig. 6a,b,c,d,f; Table S4).

The most important processes driving the biogeochemical responses to anoxia were much

456 higher fluxes of NH_4^+, DRP, and DOC into the hypolimnion from the sediments in anoxic
457 periods relative to oxic periods (Fig. 7, Fig. S5). During anoxic summer conditions, the median
458 release rates of NH_4^+ and DRP from the sediments into the water column were 3.6× and 2.2×
459 higher, respectively, than in oxic conditions (Fig. 7b,c). During oxic conditions, the sediment
460 release rate of NH_4^+ into the hypolimnion was 34× greater than the consumption of NH_4^+ by
461 nitrification (Fig. 7b), thereby explaining the hypolimnetic accumulation of NH_4^+ that occurred
462 during oxic conditions (Fig. 4g). Although median labile dissolved organic N (DON) and P
463 (DOP) mineralization rates were both 4.0× times higher in oxic than anoxic conditions, their
464 contribution to hypolimnetic N and P budgets was much smaller than NH_4^+ and DRP sediment
465 fluxes. All biogeochemical rates involving the cycling of NO_3^- were much lower than for NH_4^+
466 overall, likely because of the much lower concentrations of NO_3^- within the DIN pool (Fig. 7b).
467 For DOC, the median sediment fluxes increasing DOC in the hypolimnion were 1.9× times
468 higher in anoxic than oxic conditions (Fig. 7a). Although labile DOC mineralization rates were
469 2.0× higher in oxic than anoxic conditions, sediment flux rates were 19× higher than
470 mineralization rates, resulting in greater hypolimnetic accumulation of DOC in anoxic relative to
471 oxic periods (Fig. 4d).

472 The time scales at which C, N, and P concentrations responded to shifts in hypolimnetic
473 oxygen availability differed as a result of multiple interacting biogeochemical processes (Fig. 4,
474 Fig. 7). For example, the onset of anoxia each summer triggered rapid decreases in NO_3^- (Fig.
475 4h), due to sediment denitrification reducing NO_3^- to N_2 (Fig. 7b). Similarly, the rapid increases
476 in hypolimnetic NH_4^+ and DOC concentrations after the onset of anoxia (Fig. 4d,g) were
477 attributable to the high rates of NH_4^+ and DOC sediment release (Fig. 7a,b). In comparison,
478 hypolimnetic DRP increases in response to anoxia occurred more slowly (Fig. 4j). This

difference in time scale reflects the lower fitted value of the half-saturation constant of modeled DRP sediment fluxes (6.91 mmol m^{-3}) relative to the half-saturation constants of NH_4^+ sediment fluxes (41.25 mmol m^{-3}) and DOC sediment fluxes (93.13 mmol m^{-3}; Carey et al. 2022a). Consequently, oxygen concentrations in the hypolimnion had to decrease to near zero before anoxia stimulated an increase in DRP sediment fluxes, following Michaelis-Menten dynamics.

How does hypolimnetic anoxia affect reservoir downstream export of C, N, and P?

Overall, anoxia significantly increased downstream export of C, N, and P from FCR (Fig. 8). During the summer months, if the reservoir's hypolimnion was oxic, FCR served as a net sink for inflowing TOC and TP, decreasing the downstream export of those fractions (Fig. 8a,g). The reservoir served as a particularly important TP sink during summer oxic conditions, with 22% of inflowing TP buried in sediments, resulting in 78% of the inflowing TP exported downstream (Fig. 9). In comparison, while the reservoir was also a TOC sink in oxic conditions, only 8% of inflowing TOC was buried in sediments or removed via emission to the atmosphere, resulting in 92% export downstream (Fig. 9). However, in most anoxic summers, the reservoir became a net source of TOC and TP downstream, meaning that inflowing TOC and TP – as well as TOC and TP that were previously retained in the reservoir sediments – were released and transported out of the reservoir (Fig. 8a,g). Consequently, on average, the reservoir exported 105% of inflowing TOC and 123% of inflowing TP in anoxic conditions (Fig. 9). DOC and DRP fluxes largely mirrored the patterns of the total fractions, though DRP had much greater flux downstream overall in anoxic summers than TP (Fig. 8b,g,h).

The reservoir was a net source of TN, DIN, and NH_4^+ downstream even in oxic conditions, but this export significantly increased when the hypolimnion became anoxic in

summer (Fig. 8c,d,e). The only fraction of N that did not exhibit higher downstream export during anoxic conditions was NO_3^- (Fig. 8f). During anoxic conditions, ~100% of inflowing NO_3^- was removed due to sediment denitrification, whereas in oxic conditions, some of this NO_3^- was exported downstream along with additional NO_3^- that originated from nitrified NH_4^+ in the reservoir (Fig. 7b). Overall, the reservoir exported 204% of inflowing TN in summer oxic conditions and 553% in anoxic conditions (Fig. 9).

Aggregated across the seven years, FCR served as a small net sink of POC, PON, and POP in its sediments in both oxic and anoxic model scenarios. All particulate organic fractions exhibited significantly higher annual burial rates in anoxic scenarios than oxic scenarios, though the differences were small, especially for POP (Table S6).

Discussion

Our study provides one of the first comprehensive analyses on the effects of oxygen on multiple fractions of C, N, and P at the whole-ecosystem scale in a freshwater ecosystem. Our unprecedented 7-year field manipulation coupled with ecosystem model simulations reveals that anoxia may decrease the ability of reservoirs to serve as sinks of C, N, and P. Moreover, both the empirical data and model output demonstrate that anoxia resulted in significantly higher summer concentrations of hypolimnetic NH_4^+, DRP, and DOC and altered dissolved and total stoichiometry by factors of 2-5×. Our integrated field manipulation and modeling study provides important insight on the biogeochemical cycling of these three elements, which are already changing in many freshwaters globally due to human activities (e.g., Powers et al. 2015, Maranger et al. 2018), and likely will change substantially more in the future as the prevalence and duration of anoxia in lakes and reservoirs increase (Tranvik et al. 2009, North et al. 2014,

525 Jenny et al. 2016a, Jane et al. 2021). Below, we first examine the effects of anoxia on each
526 elemental cycle separately, then their combined stoichiometry, and ultimately whole-ecosystem
527 biogeochemical processing and fate.
528
529 *Hypolimnetic carbon and nutrient chemistry*
530 This study provides an answer to the critical question of how increased anoxia will affect
531 OC cycling at the whole-ecosystem scale (Sobek et al. 2009, Brothers et al. 2014, Peter et al.
532 2016, Mendonça et al. 2017, Carey et al. 2018). The shift in reservoir OC cycling in response to
533 anoxia is the consequence of changes in three linked processes: POC burial, DOC
534 mineralization, and DOC release from the sediments. Under anoxic conditions, POC burial
535 increased slightly, DOC mineralization rates were low, and DOC release from the sediments to
536 the water column was 2× higher than in oxic conditions (Fig. 7a, Table S6). Under oxic
537 conditions, DOC mineralization rates, while higher than in anoxic conditions (Fig. 7, Fig. S5),
538 were still an order of magnitude lower than the rate of hydrologic flushing. The net outcome of
539 these three processes was a substantial difference in OC retention in the reservoir during oxic vs.
540 anoxic conditions. Under oxic conditions, the reservoir served as a net sink of DOC and TOC,
541 with up to 18% of inflowing DOC and TOC retained in a summer (Fig. 8a,b). Under anoxic
542 conditions, the decrease in net retention of inflowing DOC and TOC more than offset the slight
543 increase in POC burial, and nearly all of the inflowing DOC and TOC was exported downstream
544 (as indicated by 0% or positive flux in Fig. 8a,b). In five of the seven years, FCR even became a
545 net exporter of TOC and DOC in the anoxic scenario (Fig. 8a,b), meaning that both inflowing
546 TOC and DOC, and likely legacy TOC and DOC that were previously buried in sediments, were
547 released and transported out of the reservoir.

548 The finding that anoxia simultaneously decreased the reservoir's role as a DOC sink yet
549 increased its role as a POC sink may explain some of the conflicting results that emerged from
550 previous studies that focused on only one OC fraction. First, our study supports past work that
551 observed increasing hypolimnetic DOC concentrations in anoxic conditions, suggesting that
552 anoxia decreases the freshwater OC sink (Brothers et al. 2014, Peter et al. 2016, Mendonça et al.
553 2017). The increasing hypolimnetic DOC concentrations have been attributed to both reductive
554 dissolution of iron-bound OC complexes in the sediments during anoxia (Skoog and Arias-
555 Esquivel 2009, Peter et al. 2016, Peter et al. 2017) and decreased mineralization rates in anoxic
556 conditions (Bastviken et al. 2004, Sobek et al. 2009). Our calibrated ecosystem model indicates
557 that both processes are important, but that the much higher hypolimnetic DOC concentrations in
558 anoxic conditions in FCR were primarily due to sediment release (Fig. 7a). At the same time, our
559 work also supports laboratory microcosm and sediment core studies that observed lower POC
560 mineralization rates in anoxic than in oxic conditions (Bastviken et al. 2004, Sobek et al. 2009).
561 In FCR, mean summer POC hydrolysis rates in the hypolimnion were five orders of magnitude
562 lower in anoxic than oxic conditions (Fig. 7a, Fig. S5), enabling slightly greater POC burial in
563 anoxic than oxic conditions. Altogether, our work indicates that using an ecosystem model to
564 simultaneously track both concentrations and rates of the major processes affecting dissolved,
565 particulate, and total pools of OC is needed to understand the full effects of oxygen on OC
566 cycling, as different fractions have different responses to anoxia.
567 Nitrogen was the most sensitive of the three focal elements to anoxia, with an NH_4^+-
568 dominated TN budget that increased dramatically during anoxic conditions. The dominant
569 mechanism driving the NH_4^+ increase in anoxic conditions were the approximately 4× higher
570 rates of ammonification and sediment release than those observed in oxic conditions (Fig. 7b).

Anammox and nitrification rates were very low in anoxic conditions (Fig. 7b, Fig. S5), enabling NH_4^+ to accumulate in the hypolimnion during anoxia. In oxic conditions, nitrification rates were unable to balance sediment fluxes, resulting in much lower but still noticeable increases in summer NH_4^+ concentrations (Fig. 4g). As a result, the reservoir functioned as an NH_4^+ source downstream regardless of hypolimnetic oxygen availability, though anoxia increased downstream fluxes by 5× relative to oxic conditions, on average. The high sediment NH_4^+ fluxes, even in oxic conditions, indicate that FCR has a large sediment NH_4^+ pool, which is likely due to historical agriculture in the catchment (Gerling et al. 2016). Until agricultural abandonment in the 1930s, most of FCR's catchment was farmland (Gerling et al. 2016). Even though the catchment did not experience industrial farming, agriculture can have century-long effects on soil properties, erosion, and ecosystem functioning (Foster et al. 2003, Cusack et al. 2013), resulting in a large pool of NH_4^+ that can be recycled between the hypolimnion and sediments for many years before eventual export (Ahlgren et al. 1994, Gerling et al. 2016).

Following expectation, hypolimnetic NO_3^- concentrations were significantly higher in oxic conditions than anoxic conditions. Despite an increase in NO_3^- during oxic conditions, the dominance of NH_4^+ over NO_3^- in the DIN pool (due to high NH_4^+ sediment fluxes even in oxic conditions; Fig. 7b) resulted in overall similar patterns for TN and NH_4^+ (Fig. 5c,d,e). We initially anticipated that an increase in NO_3^- in oxic conditions could balance an increase in NH_4^+ in anoxic conditions, thereby resulting in similar DIN concentrations regardless of oxygen level, but low nitrification rates prevented increases in NO_3^- from occurring in oxic conditions (Fig. 7b). Long-term water chemistry monitoring of FCR shows much lower summer NO_3^- concentrations over time relative to NH_4^+ (Fig. 3e,f), and thus modeled results follow observations.

Altogether, anoxia significantly decreased FCR's role as a NH_4^+ sink and simultaneously increased its role as an NO_3^- sink (Fig. 8e,f), to the extent that ~100% of inflowing NO_3^- was removed via denitrification. A previous study reported an average TN retention rate of 26% (and up to 78%) of inputs for agricultural reservoirs in the U.S. (Powers et al. 2015). It would be expected that FCR, which is located in a forested catchment, would have much higher TN retention than agricultural reservoirs because of its lower external TN loads; however, FCR's high export of NH_4^+ resulted in the reservoir serving as a source of TN downstream regardless of hypolimnetic oxygen availability (Fig. 9). We anticipate that a greater duration and prevalence of hypolimnetic anoxia in lakes and reservoirs could increase freshwater NO_3^- retention, while decreasing TN retention if a waterbody's DIN pool is dominated by NH_4^+, as in FCR.

Summer hypolimnetic DRP concentrations were approximately 3× higher in anoxic conditions than oxic conditions (Fig. 5h). DRP cycling was primarily controlled by sediment fluxes (Fig. 7c), which encompassed both release from metal complexes and sediment organic matter into the water column. Our observation of 2.2× higher sediment release rates of DRP in anoxic than oxic conditions (Fig. 7c) follows decades of work that have observed similar patterns of increased P fluxes during anoxia (Mortimer 1971, Nürnberg 1987, Boström et al. 1988, Rydin 2000, Søndergaard et al. 2003).

A novel component of our study is that we simultaneously quantified both dissolved and total pools of P at the whole-ecosystem scale in our model simulations, allowing us to disentangle the responses of different P fractions to anoxia. While DRP concentrations tripled in response to anoxia, TP concentrations only increased by 1.6× (Fig. 5g,h), indicating a lower sensitivity of particulate P than DRP to hypolimnetic oxygen conditions in FCR. This result is supported by the negligible (albeit statistically significant) response of POP to changes in oxygen

availability (Table S6). Consequently, we expect that the effects of anoxia on reservoir TP dynamics are dependent on the proportion of dissolved P vs. particulate P within the TP pool. If the hypolimnetic DRP pool comprises a sizeable proportion of TP, as observed in FCR (median of 11±1%), then TP retention will likely be sensitive to anoxia (e.g., Fig. 9), but if DRP is lower, then TP cycling may be more resilient to anoxia.

Shifts in stoichiometry in response to anoxia

The substantial difference in stoichiometric ratios between anoxic and oxic conditions has important implications for understanding how anoxia affects the ecosystem functioning of lakes and reservoirs. Because anoxia increased hypolimnetic NH_4^+ concentrations more than any other dissolved or total fraction in this study, and NH_4^+ dominated both the dissolved and total N pools, any stoichiometric ratios that included NH_4^+, DIN, or TN exhibited large shifts during anoxia (Fig. 6). The significantly higher TN:TP and DIN:DRP ratios observed during anoxia will likely affect water quality and food web structure (Fig. 6g,h). Higher N:P ratios favor non-N-fixing cyanobacteria and will shift the composition of other taxa in phytoplankton community based on their N and P requirements (Reynolds 2006), as phytoplankton can access hypolimnetic nutrients via multiple mechanisms (Cottingham et al. 2015). In contrast, the significantly lower TOC:TN, TOC:TP, DOC:DIN, DOC:NH_4^+, and DOC:DRP ratios during anoxia (Fig. 6a,b,c,d,f) could increase organic matter mineralization rates (e.g., Coble et al. 2015).

Our results both support and contradict earlier studies that measured freshwater stoichiometry across many waterbodies. Similar to an analysis of >27,000 freshwater samples from U.S. waterbodies (Helton et al. 2015), we observed inverse relationships between NO_3^- vs. NH_4^+ concentrations and DOC vs. DIN concentrations (Fig. 6). Our study provides experimental

640 evidence to support the hypothesis that redox gradients are a major driver of NO_3^-:NH_4^+ and
641 DOC:DIN ratios, which will increase in oxic conditions and decrease in anoxic conditions
642 (Helton et al. 2015). On the other hand, our work finds only partial support for earlier findings of
643 lower TOC:TP and TN:TP ratios in reservoirs than natural lakes in an analysis of ~1000 U.S.
644 waterbodies, which was attributed in part to a greater incidence of anoxia in reservoirs
645 (Maranger et al. 2018). Median TOC:TP and TN:TP ratios in the reservoirs of that study were
646 417 and 38, respectively, which are similar to the ratios observed in FCR (Fig. 6b,g). While
647 anoxia decreased TOC:TP ratios (Fig. 6b), it also increased TN:TP ratios (Fig. 6g), suggesting
648 that anoxia is not responsible for all differences in stoichiometry between reservoirs and natural
649 lakes. Our results indicate that individual waterbodies' responses to anoxia may be dependent on
650 the dominance of NO_3^- vs. NH_4^+ in their DIN pool prior to the onset of anoxia: if NO_3^-
651 dominates, then TN:TP ratios will likely decrease with anoxia, while if NH_4^+ dominates, then
652 TN:TP ratios will likely increase. In general, most lakes tend to have higher NO_3^- than NH_4^+
653 concentrations (Quirós 2003, Leoni et al. 2018), suggesting that anoxia may result in lower
654 TN:TP ratios in most waterbodies.
655
656 *Opportunities and challenges of our whole-ecosystem approach*
657 Our coupled field manipulation and modeling study provided a powerful approach for
658 quantifying freshwater ecosystem responses to anoxia. By focusing on the same reservoir
659 experiencing different oxygen conditions over multiple years, we were able to isolate the effects
660 of oxygen on C, N, and P cycling without having to disentangle ecosystem-specific responses
661 (e.g., if we were comparing across multiple waterbodies). Ideally, we would have run the
662 REDOX field manipulation with multiple summers of continuous oxygenation and multiple

663 summers of no oxygenation to contrast hypolimnetic conditions. However, we were constrained
664 in our manipulation as the reservoir was an active drinking water source during the study,
665 necessitating us to activate the oxygenation system every summer for the preservation of water
666 quality. Consequently, we used the calibrated ecosystem model to simulate the biogeochemistry
667 of continuously oxygenated and never-oxygenated scenarios, which uniquely enabled us to
668 compare the effect of oxygenation while holding all other factors constant, such as temperature
669 (Fig. 4a). The similar biogeochemical responses to anoxia between the non-oxygenated vs.
670 oxygenated field data and the anoxic vs. oxic model scenarios support our integrated study
671 approach and the robustness of our findings (e.g., Fig. 5, Fig. S2).

672 The simulation model provided insights to reservoir responses to anoxia that would have
673 been challenging to glean from field observations alone. We used the model to calculate whole-
674 ecosystem rates that are impossible to measure in the field (e.g., daily POC burial), determine the
675 relative importance of different processes for biogeochemical budgets, and quantify how
676 processes changed in anoxic vs. oxic conditions. While the model's biogeochemical rates were
677 determined from automated optimization and calibration of numerical simulation parameters,
678 they fall within reasonable ranges of biogeochemical rates observed in the field, supporting our
679 model results. For example, hypolimnetic sediment flux chamber measurements that were
680 collected in FCR in summer 2018 measured a mean sediment oxygen demand of ~20 mmol m^{-2}
681 d^{-1} (range 8-37.5 mmol m^{-2} d^{-1}), which compares well with our calibrated hypolimnetic flux of
682 29 mmol m^{-2} d^{-1} (Krueger et al. 2020). That study also measured NH_4^+, DRP, and DOC fluxes
683 from the sediment into the water column as the chambers became anoxic, with calculated release
684 rates up to 2.7 mmol NH_4^+ m^{-2} d^{-1}, 0.01 mmol DRP m^{-2} d^{-1}, and 14 mmol DOC m^{-2} d^{-1}
685 (Supporting Information Text 1). These numbers are consistent with our maximum calibrated

686 rates of 2.8 mmol NH_4^+ m^{-2} d^{-1} and 0.02 mmol DRP m^{-2} d^{-1} (Carey et al. 2022a). Our maximum
687 calibrated rate for DOC sediment flux, 1.4 mmol DOC m^{-2} d^{-1}, is an order of magnitude lower
688 than the field data, suggesting that our modeled sediment flux rate of DOC was likely
689 conservative.

690 We note several limitations to our study that should be considered. First, FCR is a small
691 reservoir (0.119 km^2). However, its size is representative of many U.S. reservoirs: 72% of the
692 reservoirs in the U.S. National Inventory of Dams have the same surface area or smaller (NID
693 2021). Second, we focused on the hypolimnion of FCR as a reactor in which we could isolate
694 coupled biogeochemical processes occurring during summer stratification, when C, N, and P
695 processing rates are usually at their highest due to warm temperatures. This focus on the
696 hypolimnion precluded the analysis of other important processes that can have large effects on
697 biogeochemical cycling in the epilimnion (e.g., photodegradation). Third, FCR has a
698 hypolimnetic withdrawal, which results in increased downstream export of hypolimnetic water
699 from the reservoir. While export of hypolimnetic water is limited in many naturally formed
700 lakes, hypolimnetic withdrawals are very common in reservoirs that provide drinking water,
701 hydropower, and flood risk protection (Hayes et al. 2017), which represent a large proportion of
702 the reservoirs in the U.S. (NID 2021). Fourth, similar to many other lake modeling studies (e.g.,
703 Kara et al. 2012, Farrell et al. 2020, Ward et al. 2020), it was challenging to model NO_3^- and
704 DRP. For these solutes in particular, most of the variation in observations was within the limit of
705 quantitation (Supporting Information Text 2), indicating that the model should not necessarily be
706 penalized for the low performance in its evaluation metrics. Despite these challenges, the N and
707 P parameters used for modeling FCR are consistent with other applications of the GLM-AED for
708 other lakes (e.g., Kara et al. 2012, Farrell et al. 2020, Ward et al. 2020), and overall, we were

generally able to recreate observed physical, chemical, and biological dynamics in both the epilimnion and hypolimnion (Fig. 3, Fig. S3, Fig. S4). Moreover, the similar results between the anoxic vs. oxic model scenarios and the field data from contrasting non-oxygenated vs. oxygenated summer days (Fig. 5, Fig. S2) support our approach and overall results.

Conclusions

The duration, prevalence, and magnitude of anoxia in the bottom waters of lakes and reservoirs are increasing globally (Butcher et al. 2015, Jenny et al. 2016a, Jane et al. 2021). While low oxygen conditions are typically thought of as a response to land use and climate change (Jenny et al. 2016b, Jane et al. 2021), our analysis demonstrates that low oxygen can also be a *driver* of major changes to freshwater biogeochemical cycling.

Importantly, our work indicates that anoxia may alter the ability of freshwater ecosystems to serve as sinks of C, N, and P in the landscape. Consequently, while hypolimnetic anoxia is a result of increased C, N, and P loading into a waterbody, we also show that it may serve as an intensifying feedback that increases anoxia in downstream waterbodies. This is evident in our study, as we found significantly higher fluxes of C, N, and P downstream when FCR was exhibiting anoxic vs. oxic conditions during the summer. Anoxia thus has the potential to both degrade the water quality of a low-oxygen waterbody as well as its downstream waterbodies. While more data are needed to evaluate the consequences of this feedback on downstream water quality, we hypothesize that it could be an important process affecting water quality in some freshwater ecosystems and necessitate greater treatment of water extracted for drinking. Given the vital role that inland waters play in removing C, N, and P from downstream export (Harrison et al. 2009, Powers et al. 2016, Maranger et al. 2018), an increased prevalence and duration of

anoxia in lakes and reservoirs will likely have major effects on global C, N, and P budgets as well as water quality and ecosystem functioning.

Acknowledgements:

We thank the Western Virginia Water Authority, especially Jamie Morris, for their long-term partnership and support. We thank Paul Gantzer, John Little, Jonathan Doubek, Kathryn Krueger, Zackary Munger, and François Birgand for assistance with REDOX, and many field and lab assistants past and present in the Reservoir Group. This work benefitted from discussions with Nelson Hairston, Jr., Emil Rydin, and Kathleen Weathers and constructive feedback from three reviewers. This study was financially supported by the National Science Foundation (DEB-1753639, DEB-1753657, CNS-1737424, DBI-1933016, DBI-1933102, DGE-1651272), Fralin Life Sciences Institute, Institute for Critical Technology and Applied Science, and Virginia Tech Global Change Center. The authors declare that they have no competing interests.

Author contributions:

Conceptualization: CCC, PCH, MES; Data curation: CCC, ABG, AGH, ASL, MEL, RPM, HLW, WMW, BRN; Formal analysis: CCC, PCH, RQT; Investigation: CCC, ABG, AGH, ASL, MEL, RPM, HLW, WMW, BRN, MES; Methodology: CCC, PCH, RQT; Project administration: CCC; Software: RQT; Visualization: CCC, ASL, RPM, WMW, AGH, HLW; Supervision: CCC, MES; Writing-original draft: CCC, MEL, BRN, AGH; Writing-review & editing: CCC, PCH, RQT, ABG, AGH, ASL, MEL, RPM, HLW, WMW, BRN, MES

754 **References**

755 Ahlgren, I., T. Waara, K. Vrede, and F. Soerensson. 1994. Nitrogen budgets in relation to
756 microbial transformations in lakes. Ambio **23**:367-377.

757 APHA. 2017. Standard Methods for the Examination of Water and Wastewater, 23rd Ed.
758 American Public Health Association, American Water Works Association, Washington
759 DC.

760 Bartosiewicz, M., A. Przytulska, J.-F. Lapierre, I. Laurion, M.F. Lehmann, and R. Maranger.
761 2019. Hot tops, cold bottoms: synergistic climate warming and shielding effects increase
762 carbon burial in lakes. Limnology and Oceanography-Letters **4**:132-144.

763 Bastviken, D., J. Cole, M. Pace, and L. Tranvik. 2004. Methane emissions from lakes:
764 Dependence of lake characteristics, two regional assessments, and a global estimate.
765 Global Biogeochemical Cycles **18**:GB4009.

766 Beaulieu, J. J., R. L. Smolenski, C. T. Nietch, A. Townsend-Small, M. S. Elovitz, and J. P.
767 Schubauer-Berigan. 2014. Denitrification alternates between a source and sink of nitrous
768 oxide in the hypolimnion of a thermally stratified reservoir. Limnology and
769 Oceanography **59**:495-506.

770 Beusen, A. H. W., A. F. Bouwman, L. P. H. Van Beek, J. M. Mogollón, and J. J. Middelburg.
771 2016. Global riverine N and P transport to ocean increased during the 20th century
772 despite increased retention along the aquatic continuum. Biogeosciences **13**:2441-2451.

773 Beutel, M., N. Burley, and K. Culmer. 2006. Quantifying the effects of water velocity and
774 oxygen on sediment oxygen demand. Hydrological Sciences & Technology **22**:271-228.

775 Beutel, M. W. 2003. Hypolimnetic anoxia and sediment oxygen demand in California drinking
776 water reservoirs. Lake and Reservoir Management **19**:208-221.

777 Boström, B., J. M. Andersen, S. Fleischer, and M. Jansson. 1988. Exchange of phosphorus
778 across the sediment-water interface. Hydrobiologia **170**:229-244.
779 Brett, M. T., S. K. Ahopelto, H. K. Brown, B. E. Brynestad, T. W. Butcher, E. E. Coba, C. A.
780 Curtis, J. T. Dara, K. B. Doeden, K. R. Evans, L. Fan, J. D. Finley, N. J. Garguilo, S. M.
781 Gebreeyesus, M. K. Goodman, K. W. Gray, C. Grinnell, K. L. Gross, B. R. E. Hite, A. J.
782 Jones, P. T. Kenyon, A. M. Klock, R. E. Koshy, A. M. Lawler, M. Lu, L. Martinkosky, J.
783 R. Miller-Schulze, Q. T. N. Nguyen, E. R. Runde, J. M. Stultz, S. Wang, F. P. White, C.
784 H. Wilson, A. S. Wong, S. Y. Wu, P. G. Wurden, T. R. Young, and G. B. Arhonditsis
785 2016. The modeled and observed response of Lake Spokane hypolimnetic dissolved
786 oxygen concentrations to phosphorus inputs. Lake and Reservoir Management **32**:246-
787 258.
788 Brothers, S., J. Köhler, K. Attermeyer, H. P. Grossart, T. Mehner, N. Meyer, K. Scharnweber,
789 and S. Hilt. 2014. A feedback loop links brownification and anoxia in a temperate,
790 shallow lake. Limnology and Oceanography **59**:1388-1398.
791 Bruce, L., M. Frassl, G. Arhonditsis, G. Gal, D. Hamilton, P. Hanson, A. Hetherington, J.
792 Melack, J. Read, K. Rinke, A. Rigosi, D. Trolle, L. Winslow, R. Adrian, A. Ayala
793 Zamora, S. Bocaniov, B. Boehrer, C. Boon, J. Brookes, and M. Hipsey. 2018. A multi-
794 lake comparative analysis of the General Lake Model (GLM): Stress-testing across a
795 global observatory network. Environmental Modelling and Software **102**:274-291.
796 Butcher, J. B., D. Nover, T. E. Johnson, and C. M. Clark. 2015. Sensitivity of lake thermal and
797 mixing dynamics to climate change. Climatic Change **129**:295-305.

798 Carey, C. C., J. P. Doubek, R. P. McClure, and P. C. Hanson. 2018. Oxygen dynamics control
799 the burial of organic carbon in a eutrophic reservoir. Limnology and Oceanography
800 Letters **3**:293-301.
801 Carey, C. C., J. P. Doubek, J. H. Wynne, and B. R. Niederlehner. 2020. Dissolved silica time
802 series for Beaverdam Reservoir, Carvins Cove Reservoir, Claytor Lake, Falling Creek
803 Reservoir, Gatewood Reservoir, Smith Mountain Lake, and Spring Hollow Reservoir in
804 southwestern Virginia, USA during 2014, ver 1. Environmental Data Initiative
805 Repository. https://doi.org/10.6073/pasta/353aa34bedfd68800c12275633811341
806 Carey, C. C., A. G. Hounshell, M. E. Lofton, B. Birgand, B. J. Bookout, R. S. Corrigan, A. B.
807 Gerling, R. P. McClure, and W. M. Woelmer. 2021a. Discharge time series for the
808 primary inflow tributary entering Falling Creek Reservoir, Vinton, Virginia, USA 2013-
809 2021, ver 7. Environmental Data Initiative repository.
810 https://doi.org/10.6073/pasta/8d22a432aac5560b0f45aa1b21ae4746
811 Carey, C. C., A. S. Lewis, R. P. McClure, A. B. Gerling, S. Chen, A. Das, J. P. Doubek, D. W.
812 Howard, M. E. Lofton, K. D. Hamre, and H. L. Wander. 2021b. Time series of high-
813 frequency profiles of depth, temperature, dissolved oxygen, conductivity, specific
814 conductivity, chlorophyll a, turbidity, pH, oxidation-reduction potential, photosynthetic
815 active radiation, and descent rate for Beaverdam Reservoir, Carvins Cove Reservoir,
816 Falling Creek Reservoir, Gatewood Reservoir, and Spring Hollow Reservoir in
817 Southwestern Virginia, USA 2013-2020, ver 11. Environmental Data Initiative
818 repository. https://doi.org/10.6073/pasta/5448f9d415fd09e0090a46b9d4020ccc
819 Carey, C. C., R. Q. Thomas, and P. C. Hanson. 2022a. General Lake Model-Aquatic
820 EcoDynamics model parameter set for Falling Creek Reservoir, Vinton, Virginia, USA

2013-2019 ver 1. Environmental Data Initiative repository. https://doi.org/10.6073/pasta/9f7d037d9a133076a0a0d123941c6396.

Carey, C. C., R. Q. Thomas, R. P. McClure, A. G. Hounshell, W. M. Woelmer, H. L. Wander, and A. S. L. Lewis. 2022b. CareyLabVT/FCR-GLM: FCR GLM-AED model, data, and code for the paper "Anoxia decreases the magnitude of the carbon, nitrogen, and phosphorus sink in freshwaters" in Global Change Biology by Carey et al. (v1.2). Zenodo. https://doi.org/10.5281/zenodo.6520742

Carey, C. C., H. L. Wander, W. M. Woelmer, M. E. Lofton, A. Breef-Pilz, J. P. Doubek, A. B. Gerling, A. G. Hounshell, R. P. McClure, and B. R. Niederlehner. 2021c. Water chemistry time series for Beaverdam Reservoir, Carvins Cove Reservoir, Falling Creek Reservoir, Gatewood Reservoir, and Spring Hollow Reservoir in southwestern Virginia, USA 2013-2020, ver 8. Environmental Data Initiative repository. https://doi.org/10.6073/pasta/8d83ef7ec202eca9192e3da6dd34a4e0

Carey, C. C., W. M. Woelmer, J. T. Maze, and A. G. Hounshell. 2019. Manually-collected discharge data for multiple inflow tributaries entering Falling Creek Reservoir and Beaverdam Reservoir, Vinton, Virginia, USA in 2019, ver 4. Environmental Data Initiative repository. https://doi.org/10.6073/pasta/4d8e7b7bedbc6507b307ba2d5f2cf9a2

Carey, C. C., J. H. Wynne, H. L. Wander, R. P. McClure, K. J. Farrell, A. Breef-Pilz, J. P. Doubek, A. B. Gerling, K. D. Hamre, A. G. Hounshell, A. S. Lewis, M. E. Lofton, and W. M. Woelmer. 2021d. Secchi depth data and discrete depth profiles of photosynthetically active radiation, temperature, dissolved oxygen, and pH for Beaverdam Reservoir, Carvins Cove Reservoir, Falling Creek Reservoir, Gatewood Reservoir, and Spring Hollow Reservoir in southwestern Virginia, USA 2013-2020, ver

844 8. Environmental Data Initiative repository.
845 https://doi.org/10.6073/pasta/3e9f27971e353c8a80840b5e99a67d0c
846 Coble, A., A. Marcarelli, and E. Kane. 2015. Ammonium and glucose amendments stimulate
847 dissolved organic matter mineralization in a Lake Superior tributary. Journal of Great
848 Lakes Research **41**:801-807.
849 Cole, J. J. 2013. Freshwater Ecosystems and the Carbon Cycle. Kinne, O., ed. Excellence in
850 Ecology, vol. 18. International Ecology Institute, Obendorf, Germany.
851 Cottingham, K. L., H. A. Ewing, M. L. Greer, C. C. Carey, and K. C. Weathers. 2015.
852 Cyanobacteria as biological drivers of lake nitrogen and phosphorus cycling. Ecosphere
853 **6**:art1. DOI: 10.1890/ES14-00174.1
854 Cusack, D. F., O. A. Chadwick, T. Ladefoged, and P. M. Vitousek. 2013. Long-term effects of
855 agriculture on soil carbon pools and carbon chemistry along a Hawaiian environmental
856 gradient. Biogeochemistry **112**:229-243.
857 Dillon, P. J., and L. A. Molot. 1997. Dissolved organic and inorganic carbon mass balances in
858 central Ontario lakes. Biogeochemistry **36**:29-42.
859 Downes, M. T. 1987. Aquatic nitrogen transformations at low oxygen concentrations. Applied
860 and Environmental Microbiology **54**:172-175.
861 Downing, J. A., Y. T. Prairie, J. J. Cole, C. M. Duarte, L. J. Tranvik, R. G. Striegl, W. H.
862 McDowell, P. Kortelainen, N. F. Caraco, J. M. Melack, and J. J. Middelburg. 2006. The
863 global abundance and size distribution of lakes, ponds, and impoundments. Limnology
864 and Oceanography **51**:2388-2397.

865 Farrell, K. J., N. K. Ward, A. I. Krinos, P. C. Hanson, V. Daneshmand, R. J. Figueiredo, and C.
866 C. Carey. 2020. Ecosystem-scale nutrient cycling responses to increasing air
867 temperatures vary with lake trophic state. Ecological Modelling **430**:109134.
868 Foster, D., F. Swanson, J. Aber, I. Burke, N. Brokaw, D. Tilman, and A. Knapp. 2003. The
869 importance of land-use legacies to ecology and conservation. Bioscience **53**:77-88.
870 Frindte, K., M. Allgaier, H.-P. Grossart, and W. Eckert. 2015. Microbial response to
871 experimentally controlled redox transitions at the sediment water interface. PLoS One
872 **10**:e0143428.
873 Gerling, A., R. Browne, P. Gantzer, M. Mobley, J. Little, and C. Carey. 2014. First report of the
874 successful operation of a side stream supersaturation hypolimnetic oxygenation system in
875 a eutrophic, shallow reservoir. Water Research **67**:129-143.
876 Gerling, A. B., Z. W. Munger, J. P. Doubek, K. D. Hamre, P. A. Gantzer, J. C. Little, and C. C.
877 Carey. 2016. Whole-catchment manipulations of internal and external loading reveal the
878 sensitivity of a century-old reservoir to hypoxia. Ecosystems **19**:555-571.
879 Hansen, N. 2016. The CMA evolution strategy: A tutorial. ArXiv **160400772**.
880 https://arxiv.org/abs/1604.00772
881 Hanson, P. C., M. L. Pace, S. R. Carpenter, J. J. Cole, and E. H. Stanley. 2015. Integrating
882 landscape carbon cycling: research needs for resolving organic carbon budgets of lakes.
883 Ecosystems **18**:363-375.
884 Harrison, J. A., R. J. Maranger, R. B. Alexander, A. E. Giblin, P.-A. Jacinthe, E. Mayorga, S. P.
885 Seitzinger, D. J. Sobota, and W. M. Wollheim. 2009. The regional and global
886 significance of nitrogen removal in lakes and reservoirs. Biogeochemistry **93**:143-157.

887 Hayes, N. M., B. R. Deemer, J. R. Corman, N. R. Razavi, and K. E. Strock. 2017. Key
888 differences between lakes and reservoirs modify climate signals: A case for a new
889 conceptual model. Limnology and Oceanography-Letters **2**:47-62.
890 Helton, A. M., M. Ardón, and E. S. Bernhardt. 2015. Thermodynamic constraints on the utility
891 of ecological stoichiometry for explaining global biogeochemical patterns. Ecology
892 Letters **18**:1049-1056.
893 Hipsey, M. R. 2022. Modelling Aquatic Eco-Dynamics: Overview of the AED modular
894 simulation platform (v0.9.0). Zenodo. https://doi.org/10.5281/zenodo.6516222
895 Hipsey, M. R., L. C. Bruce, C. Boon, B. Busch, C. C. Carey, D. P. Hamilton, P. C. Hanson, J. S.
896 Read, E. de Sousa, M. Weber, and L. A. Winslow. 2019. A General Lake Model (GLM
897 3.0) for linking with high-frequency sensor data from the Global Lake Ecological
898 Observatory Network (GLEON). Geoscience Model Development **12**:473-523.
899 Hounshell, A. G., R. P. McClure, M. E. Lofton, and C. C. Carey. 2021. Whole-ecosystem
900 oxygenation experiments reveal substantially greater hypolimnetic methane
901 concentrations in reservoirs during anoxia. **6**:33-42.
902 Jane, S. F., G. J. A. Hansen, B. M. Kraemer, P. R. Leavitt, J. L. Mincer, R. L. North, R. M. Pilla,
903 J. T. Stetler, C. E. Williamson, R. I. Woolway, L. Arvola, S. Chandra, C. L. DeGasperi,
904 L. Diemer, J. Dunalska, O. Erina, G. Flaim, H.-P. Grossart, K. D. Hambright, C. Hein, J.
905 Hejzlar, L. L. Janus, J.-P. Jenny, J. R. Jones, L. B. Knoll, B. Leoni, E. Mackay, S.-I. S.
906 Matsuzaki, C. McBride, D. C. Müller-Navarra, A. M. Paterson, D. Pierson, M. Rogora, J.
907 A. Rusak, S. Sadro, E. Saulnier-Talbot, M. Schmid, R. Sommaruga, W. Thiery, P.
908 Verburg, K. C. Weathers, G. A. Weyhenmeyer, K. Yokota, and K. C. Rose. 2021.
909 Widespread deoxygenation of temperate lakes. Nature **594**:66-70.

910 Jenny, J.-P., P. Francus, A. Normandeau, F. Lapointe, M.-E. Perga, A. Ojala, A. Schimmelmann,
911 and B. Zolitschka. 2016a. Global spread of hypoxia in freshwater ecosystems during the
912 last three centuries is caused by rising local human pressure. Global Change Biology
913 **22**:1481-1489.
914 Jenny, J.-P., A. Normandeau, P. Francus, Z. E. Taranu, I. Gregory-Eaves, F. Lapointe, J. Jautzy,
915 A. E. K. Ojala, J.-M. Dorioz, A. Schimmelmann, and B. Zolitschka. 2016b. Urban point
916 sources of nutrients were the leading cause for the historical spread of hypoxia across
917 European lakes. Proceedings of the National Academy of Sciences **113**:12655.
918 Kara, E. L., P. Hanson, D. Hamilton, M. R. Hipsey, K. D. McMahon, J. S. Read, L. Winslow, J.
919 Dedrick, K. Rose, C. C. Carey, S. Bertilsson, D. da Motta Marques, L. Beversdorf, T.
920 Miller, C. Wu, Y.-F. Hsieh, E. Gaiser, and T. Kratz. 2012. Time-scale dependence in
921 numerical simulations: Assessment of physical, chemical, and biological predictions in a
922 stratified lake at temporal scales of hours to months. Environmental Modelling &
923 Software **35**:104-121.
924 Kim, C., Y. Nishimura, and T. Nagata. 2006. Role of dissolved organic matter in hypolimnetic
925 mineralization of carbon and nitrogen in a large, monomictic lake. Limnology and
926 Oceanography **51**:70-78.
927 Kortelainen, P., M. Rantakari, H. Pajunen, J. T. Huttunen, T. Mattsson, J. Alm, S. Juutinen, T.
928 Larmola, J. Silvola, and P. J. Martikainen. 2013. Carbon evasion/accumulation ratio in
929 boreal lakes is linked to nitrogen. Global Biogeochemical Cycles **27**:363-374.
930 Krueger, K. M., C. E. Vavrus, M. E. Lofton, R. P. McClure, P. Gantzer, C. C. Carey, and M. E.
931 Schreiber. 2020. Iron and manganese fluxes across the sediment-water interface in a
932 drinking water reservoir. Water Research **182**:116003.

933 Ladwig, R., P. C. Hanson, H. A. Dugan, C. C. Carey, Y. Zhang, L. Shu, C. J. Duffy, and K. M.
934 Cobourn. 2021. Lake thermal structure drives interannual variability in summer anoxia
935 dynamics in a eutrophic lake over 37 years. Hydrology and Earth System Science
936 **25**:1009-1032.
937 Lau, M. P., M. Sander, J. Gelbrecht, and M. Hupfer. 2016. Spatiotemporal redox dynamics in a
938 freshwater lake sediment under alternating oxygen availabilities: combined analyses of
939 dissolved and particulate electron acceptors. Environmental Chemistry **13**:826-837.
940 Lehner, B., C. R. Liermann, C. Revenga, C. Vörösmarty, B. Fekete, P. Crouzet, P. Döll, M.
941 Endejan, K. Frenken, J. Magome, C. Nilsson, J. C. Robertson, R. Rödel, N. Sindorf, and
942 D. Wisser. 2011. High-resolution mapping of the world's reservoirs and dams for
943 sustainable river-flow management. Frontiers in Ecology and the Environment **9**:494-
944 502.
945 Leoni, B., M. Patelli, V. Soler, and V. Nava. 2018. Ammonium transformation in 14 lakes along
946 a trophic gradient. Water **10**. DOI: 10.3390/w10030265
947 Maranger, R., S. E. Jones, and J. B. Cotner. 2018. Stoichiometry of carbon, nitrogen, and
948 phosphorus through the freshwater pipe. Limnology and Oceanography Letters **3**:89-101.
949 McDonald, C. P., E. G. Stets, R. G. Striegl, and D. Butman. 2013. Inorganic carbon loading as a
950 primary driver of dissolved carbon dioxide concentrations in the lakes and reservoirs of
951 the contiguous United States. Global Biogeochemical Cycles **27**:285-295.
952 Medlyn, B. E., S. Zaehle, M. G. De Kauwe, A. P. Walker, M. C. Dietze, P. J. Hanson, T.
953 Hickler, A. K. Jain, Y. Luo, W. Parton, I. C. Prentice, P. E. Thornton, S. Wang, Y.-P.
954 Wang, E. Weng, C. M. Iversen, H. R. McCarthy, J. M. Warren, R. Oren, and R. J. Norby.

2015. Using ecosystem experiments to improve vegetation models. Nature Climate Change **5**:528-534.

Mendonça, R., R. A. Müller, D. Clow, C. Verpoorter, P. Raymond, L. J. Tranvik, and S. Sobek. 2017. Organic carbon burial in global lakes and reservoirs. Nature Communications **8**:1694.

Morris, M. D. 1991. Factorial sampling plans for preliminary computational experiments. Technometrics **33**:161-174.

Mortimer, C. H. 1971. Chemical exchanges between sediments and water in the Great Lakes - speculations on probable regulatory mechanisms. Limnology and Oceanography **16**:387-404.

Munger, Z. W., C. C. Carey, A. B. Gerling, J. P. Doubek, K. D. Hamre, R. P. McClure, and M. E. Schreiber. 2019. Oxygenation and hydrologic controls on iron and manganese mass budgets in a drinking-water reservoir. Lake and Reservoir Management **35**:277-291.

NID 2021. U.S. National Inventory of Dams. Washington, DC: US Army Corps of Engineers. https://nid.usace.army.mil/#/ Accessed on 2021-12-31.

North, R. P., R. L. North, D. M. Livingstone, O. Köster, and R. Kipfer. 2014. Long-term changes in hypoxia and soluble reactive phosphorus in the hypolimnion of a large temperate lake: consequences of a climate regime shift. Global Change Biology **20**:811-823.

Nürnberg, G. K. 1987. A comparison of internal phosphorus loads in lakes with anoxic hypolimnia. Limnology and Oceanography **32**:1160-1164.

Nürnberg, G. K. 1988. Prediction of phosphorus release rates from total and reductant-soluble phosphorus in anoxic lake sediments. Canadian Journal of Fisheries and Aquatic Sciences **45**:453-462.

978 Peter, S., O. Agstam, and S. Sobek. 2017. Widespread release of dissolved organic carbon from
979 anoxic boreal lake sediments. Inland Waters **7**:151-163.
980 Peter, S., A. Isidorova, and S. Sobek. 2016. Enhanced carbon loss from anoxic lake sediment
981 through diffusion of dissolved organic carbon. Journal of Geophysical Research:
982 Biogeosciences **121**:1959-1977.
983 Powers, S. M., T. W. Bruulsema, T. P. Burt, N. I. Chan, J. J. Elser, P. M. Haygarth, N. J. K.
984 Howden, H. P. Jarvie, Y. Lyu, H. M. Peterson, Andrew N. Sharpley, J. Shen, F. Worrall,
985 and F. Zhang. 2016. Long-term accumulation and transport of anthropogenic phosphorus
986 in three river basins. Nature Geoscience **9**:353-356.
987 Powers, S. M., J. L. Tank, and D. M. Robertson. 2015. Control of nitrogen and phosphorus
988 transport by reservoirs in agricultural landscapes. Biogeochemistry **124**:417-439.
989 Quirós, R. 2003. The relationship between nitrate and ammonia concentrations in the pelagic
990 zone of lakes. Limnetica **22**:37-50.
991 Rydin, E. 2000. Potentially mobile phosphorus in Lake Erken sediment. Water Research
992 **34**:2037-2042.
993 Rysgaard, S., N. Risgaard-Petersen, N. Sloth, K. I. M. Jensen, and L. P. Nielsen. 1994. Oxygen
994 regulation of nitrification and denitrification in sediments. Limnology and Oceanography
995 **39**:1643-1652.
996 Sharma, B., and R. C. Ahlert. 1977. Nitrification and nitrogen removal. Water Research **11**:897-
997 925.
998 Skoog, A. C., and V. A. Arias-Esquivel. 2009. The effect of induced anoxia and reoxygenation
999 on benthic fluxes of organic carbon, phosphate, iron, and manganese. Science of the
1000 Total Environment **407**:6085-6092.

1001 Soares, L. M. V., and M. d. C. Calijuri. 2021. Deterministic modelling of freshwater lakes and
1002 reservoirs: Current trends and recent progress. Environmental Modelling & Software
1003 **144**:105143.
1004 Sobek, S., E. Durisch-Kaiser, R. Zurbrügg, N. Wongfun, M. Wessels, N. Pasche, and B. Wehrli.
1005 2009. Organic carbon burial efficiency in lake sediments controlled by oxygen exposure
1006 time and sediment source. Limnology and Oceanography **54**:2243-2254.
1007 Søndergaard, M., J. P. Jensen, and E. Jeppesen. 2003. Role of sediment and internal loading of
1008 phosphorus in shallow lakes. Hydrobiologia **506**:135-145.
1009 Sterner, R., and J. J. Elser. 2002. Ecological Stoichiometry: The Biology of Elements From
1010 Molecules to The Biosphere. Princeton University Press, Princeton, NJ.
1011 R Core Team. 2020. R: A language and environment for statistical computing. Version 3.6.3. R
1012 Foundation for Statistical Computing, Vienna, Austria.
1013 Toming, K., J. Kotta, E. Uuemaa, S. Sobek, T. Kutser, and L. J. Tranvik. 2020. Predicting lake
1014 dissolved organic carbon at a global scale. Scientific Reports **10**:8471.
1015 Tranvik, L. J., J. A. Downing, J. B. Cotner, S. A. Loiselle, R. G. Striegl, T. J. Ballatore, P.
1016 Dillon, K. Finlay, K. Fortino, L. B. Knoll, P. L. Kortelainen, T. Kutser, S. Larsen, I.
1017 Laurion, D. M. Leech, S. L. McCallister, D. M. McKnight, J. M. Melack, E. Overholt, J.
1018 A. Porter, Y. Prairie, W. H. Renwick, F. Roland, B. S. Sherman, D. W. Schindler, S.
1019 Sobek, A. Tremblay, M. J. Vanni, A. M. Verschoor, E. von Wachenfeldt, and G. A.
1020 Weyhenmeyer. 2009. Lakes and reservoirs as regulators of carbon cycling and climate.
1021 Limnology and Oceanography **54**:2298-2314.

1022 Vachon, D., T. Langenegger, D. Donis, and D. F. McGinnis. 2019. Influence of water column
1023 stratification and mixing patterns on the fate of methane produced in deep sediments of a
1024 small eutrophic lake. Limnology and Oceanography **64**:2114–2128.
1025 Verpoorter, C., T. Kutser, D. A. Seekell, and L. J. Tranvik. 2014. A global inventory of lakes
1026 based on high-resolution satellite imagery. Geophysical Research Letters **41**:6396-6402.
1027 Walker, R. R., and W. J. Snodgrass. 1986. Model for sediment oxygen demand in lakes. Journal
1028 of Environmental Engineering **112**:25-43.
1029 Ward, N. K., B. G. Steele, K. C. Weathers, K. L. Cottingham, H. A. Ewing, P. C. Hanson, and C.
1030 C. Carey. 2020. Differential responses of maximum versus median chlorophyll-a to air
1031 temperature and nutrient loads in an oligotrophic lake over 31 years. Water Resources
1032 Research **56**:e2020WR027296.
1033 Wetzel, R. G. 2001. Limnology: Lake and River Ecosystems. 3rd edition. Academic Press, New
1034 York.
1035 Woolway, R. I., S. Sharma, G. A. Weyhenmeyer, A. Debolskiy, M. Golub, D. Mercado-Bettín,
1036 M. Perroud, V. Stepanenko, Z. Tan, L. Grant, R. Ladwig, J. Mesman, T. N. Moore, T.
1037 Shatwell, I. Vanderkelen, J. A. Austin, C. L. DeGasperi, M. Dokulil, S. La Fuente, E. B.
1038 Mackay, S. G. Schladow, S. Watanabe, R. Marcé, D. C. Pierson, W. Thiery, and E.
1039 Jennings. 2021. Phenological shifts in lake stratification under climate change. Nature
1040 Communications **12**:2318.
1041 Xia, Y., K. Mitchell, M. Ek, J. Sheffield, B. Cosgrove, E. Wood, L. Luo, C. Alonge, H. Wei, J.
1042 Meng, B. Livneh, D. Lettenmaier, V. Koren, Q. Duan, K. Mo, Y. Fan, and D. Mocko.
1043 2012. Continental-scale water and energy flux analysis and validation for the North
1044 American Land Data Assimilation System project phase 2 (NLDAS-2): 1.

1045 Intercomparison and application of model products. Journal of Geophysical Research:
1046 Atmospheres **117**:D03109.
1047 Zarfl, C., A. E. Lumsdon, J. Berlekamp, L. Tydecks, and K. Tockner. 2015. A global boom in
1048 hydropower dam construction. Aquatic Sciences **77**:161-170.
1049
1050

Table 1. Goodness-of-fit (GOF) metrics for comparing observations and modeled GLM-AED output for Falling Creek Reservoir, VA, USA. GOF metrics include root mean square error (RMSE), percent bias (PBIAS%), coefficient of determination (R^2), and normalized mean absolute error (NMAE); *n* is the number of observed measurements. Each GOF metric was calculated comparing model outputs and observational data for the water column for the Full simulation (2013-2019); Calibration (2013-2018); and Validation (2018-2019); see Supporting Information Text 3 for details. Evaluated parameters include temperature (Temp, ºC), summer thermocline depth (TD, m), dissolved oxygen (mmol m^{-3}), dissolved organic carbon (DOC, mmol m^{-3}), total nitrogen (TN, mmol m^{-3}), ammonium (NH_4^+, mmol m^{-3}), nitrate (NO_3^-, mmol m^{-3}), total phosphorus (TP, mmol m^{-3}), and dissolved reactive phosphorus (DRP, mmol m^{-3}).

Time period	**Parameter**	**Temp**	**TD**	**Oxygen**	**DOC**	**TN**	**NH_4^+**	**NO_3^-**	**TP**	**DRP**
Full simulation	*n*	3639	324	3726	1277	1518	1277	1485	1724	1271
	RMSE	1.41	0.8	49.1	63.2	5.9	2.81	0.16	0.29	0.05
	PBIAS%	4.4	0.1	6.4	-14.5	-6.2	22.5	9.8	-31.7	26.5
	R^2	0.95	0.50	0.72	0.30	0.71	0.77	0.27	0.25	0.10
	NMAE	0.09	0.18	0.15	0.2	0.22	0.46	0.45	0.38	0.37
Calibration	*n*	3164	284	3251	1018	1250	1018	1014	1456	1012
	RMSE	1.39	0.9	45.9	61.5	5.0	2.81	0.16	0.25	0.04
	PBIAS%	3.3	-1.4	5.8	-16.8	-0.8	40.7	11.7	-29.6	21.1
	R^2	0.95	0.46	0.71	0.46	0.58	0.63	0.33	0.15	0.24
	NMAE	0.09	0.19	0.14	0.19	0.19	0.61	0.44	0.33	0.28
Validation	*n*	475	40	475	259	268	259	471	268	259
	RMSE	1.48	0.4	62.8	70.4	9.23	2.79	0.14	0.33	0.08
	PBIAS%	11.2	10.5	9.9	-4.2	-19.8	-7.2	3.3	-42.9	51.6
	R^2	0.97	0.95	0.74	0.52	0.94	0.94	0.12	0.85	0.03
	NMAE	0.12	0.1	0.2	0.24	0.36	0.22	0.49	0.38	0.57

Figure legends

Fig. 1. Conceptual diagram of the dominant carbon, nitrogen, and phosphorus cycling processes in oxic (top) and anoxic (bottom) conditions in the water column of a thermally stratified reservoir. Carbon processes include cycling of carbon dioxide (CO_2), dissolved organic carbon (DOC), methane (CH_4), and particulate organic carbon (POC). Nitrogen processes include cycling of dissolved organic nitrogen (DON), nitrogen gas (N_2), ammonium (NH_4^+), nitrate (NO_3^-), and particulate organic nitrogen (PON). Phosphorus processes include cycling of dissolved organic phosphorus (DOP), dissolved reactive phosphorus (DRP), and particulate organic phosphorus (POP). Processes are denoted by arrows.

Fig. 2. Map of Falling Creek Reservoir, Vinton, VA, USA (37.303479, -79.837371). The map shows the reservoir watershed, locations of the two inflow streams (Falling Creek and Tunnel Branch), dam, hypolimnetic oxygenation (HOx) system, and monitoring site near the dam.

Fig. 3. The model was able to generally recreate observed reservoir dynamics. Modeled (black line) and observed (red points) hypolimnetic (9 m) water temperature (a), dissolved oxygen (b), dissolved organic carbon (DOC; c), total nitrogen (TN; d), ammonium (NH_4^+; e), nitrate (NO_3^-; f), total phosphorus (TP; g), and dissolved reactive phosphorus (DRP; h) in Falling Creek Reservoir (goodness-of-fit metrics presented for the full water column in Table 1). The grey shaded areas in panel (b) represent the periods and addition rates of oxygen injection into the hypolimnion from the hypolimnetic oxygenation system (HOx) during the seven-year field manipulation. Note varying y-axes among panels, and that many of the NO_3^- and DRP observations were below the limit of quantitation in laboratory analysis (0.11 and 0.08 mmol m^{-3}, respectively).

Fig. 4. Time series of oxic (blue) and anoxic (red) model scenarios in Falling Creek Reservoir. Model results are shown for hypolimnetic (9 m) water temperature (a), dissolved oxygen (b), total organic carbon (TOC; c), dissolved organic carbon (DOC; d), total nitrogen (TN; e), dissolved inorganic nitrogen (DIN, the sum of ammonium and nitrate; f), ammonium (NH_4^+; g), nitrate (NO_3^-; h), total phosphorus (TP; i), and dissolved reactive phosphorus (DRP; j). In the oxic scenario, oxygen was injected into the hypolimnion throughout the thermally stratified period each summer. In the anoxic scenario, no oxygen was added to the hypolimnion, resulting in prolonged hypolimnetic anoxia each summer. Note varying y-axes among panels.

Fig. 5. Anoxia significantly altered bottom-water concentrations of carbon, nitrogen, and phosphorus. Median hypolimnetic (9 m) total organic carbon (TOC; a), dissolved organic carbon (DOC; b), total nitrogen (TN; c), dissolved inorganic nitrogen (DIN; d), ammonium (NH_4^+; e), nitrate (NO_3^-; f), total phosphorus (TP; g), and dissolved reactive phosphorus (DRP; h) concentrations between anoxic (red) and oxic (blue) scenarios during Falling Creek Reservoir's stratified period (July 15 - October 1) for all years of this study. The grey points are the median values from each of the seven years. The **** denotes that the difference between the median summer anoxic and oxic scenario concentrations was highly statistically significant (all paired t-tests $p \leq 0.0001$, see Table S3 for statistics). Note varying y-axes among panels.

Fig. 6. Anoxia significantly affected water column stoichiometry. Total and dissolved molar ratios of hypolimnetic (9 m) total organic carbon:total nitrogen (TOC:TN; a), TOC:total phosphorus (TOC:TP; b), dissolved organic carbon:dissolved inorganic nitrogen (DOC:DIN; c), DOC:ammonium (DOC:NH_4^+; d), DOC:nitrate (DOC:NO_3^-; e), DOC:dissolved reactive phosphorus (DOC:DRP; f), TN:TP (g), and DIN:DRP (h) between anoxic (red) and oxic (blue) scenarios during Falling Creek Reservoir's stratified period (July 15 - October 1) for all years of this study. The grey points are the median values from each of the seven years. Because NO_3^- concentrations in the anoxic scenario were functionally zero, the ratio of DOC:NO_3^- could not be calculated (hence the X in panel e). The asterisks denote the p-values from paired t-tests comparing the median summer ratios between anoxic and oxic scenarios: **** $p < 0.0001$, *** $p < 0.001$, ** $p < 0.01$, and * $p < 0.05$ (see Table S4 for statistics). Note varying y-axes among panels.

Fig. 7. Sediment fluxes dominated the responses of dissolved carbon, nitrogen, and phosphorus to anoxia. Comparison of the dominant biogeochemical processes altering dissolved pools of carbon (dissolved organic carbon, DOC; a), nitrogen (ammonium, NH_4^+, and nitrate, NO_3^-; b), and phosphorus (dissolved reactive phosphorus, DRP; c) in the hypolimnion of Falling Creek Reservoir under anoxic vs. oxic model scenarios. Rates shown represent the median contribution of each process to hypolimnetic concentrations of DOC, NH_4^+, NO_3^-, and DRP during Falling Creek Reservoir's summer stratified period (July 15 - October 1) for all years of this study. Positive rates indicate that the process increased hypolimnetic concentrations; negative rates indicate that the process decreased hypolimnetic concentrations. Mineralization is shown separately for both labile (labl.) and recalcitrant (recalc.) dissolved organic pools, and denitrification is partitioned for the water column (WC denitrification) and sediment in the NO_3^- panel (Sediment flux). Note the varying y-axes among panels and that some rates are so small that they are not visible in the figure; Fig. S5 shows a modified version of this figure with the sediment fluxes excluded.

Fig. 8. Anoxia significantly increased the downstream export of carbon, nitrogen, and phosphorus. Percent downstream export (% flux) of total organic carbon (TOC; a), dissolved organic carbon (DOC; b), total nitrogen (TN; c), dissolved inorganic nitrogen (DIN; d), ammonium (NH_4^+; e), nitrate (NO_3^-; f), total phosphorus (TP; g), and dissolved reactive phosphorus (DRP; h) inputs into Falling Creek Reservoir for anoxic (red) and oxic (blue) model scenarios during the stratified period (July 15 - October 1) for all years of this study. Flux values of 0 (denoted by dashed horizontal lines) indicated that the reservoir inputs balanced exports; flux values <0 indicated that the reservoir was a net sink of C, N, or P; and flux values >0 indicated that the reservoir was a net source of C, N, or P downstream. The grey points are the median values from each of the seven years. The asterisks denote the p-values from paired t-tests comparing the median summer retention in anoxic and oxic scenarios: **** $p < 0.0001$, *** $p < 0.001$, and ** $p < 0.01$ (see Table S5 for statistics). Note varying y-axes among panels.

Fig. 9. Median summer downstream export of total organic carbon (C), total nitrogen (N), and total phosphorus (P) inputs under oxic (top) and anoxic (bottom) conditions. The "% of inflow" value represents the percent of inflowing C, N, and P into the reservoir that is exported downstream. A value of 100% indicates that reservoir inputs balanced exports; values <100% indicated that the reservoir was a net sink of C, N, or P; and values >100% indicated that the

1153 reservoir was a net source of C, N, or P downstream. Arrow widths are scaled to be proportional
1154 to the median downstream export of each element.
1155

1156 **Fig. 1**

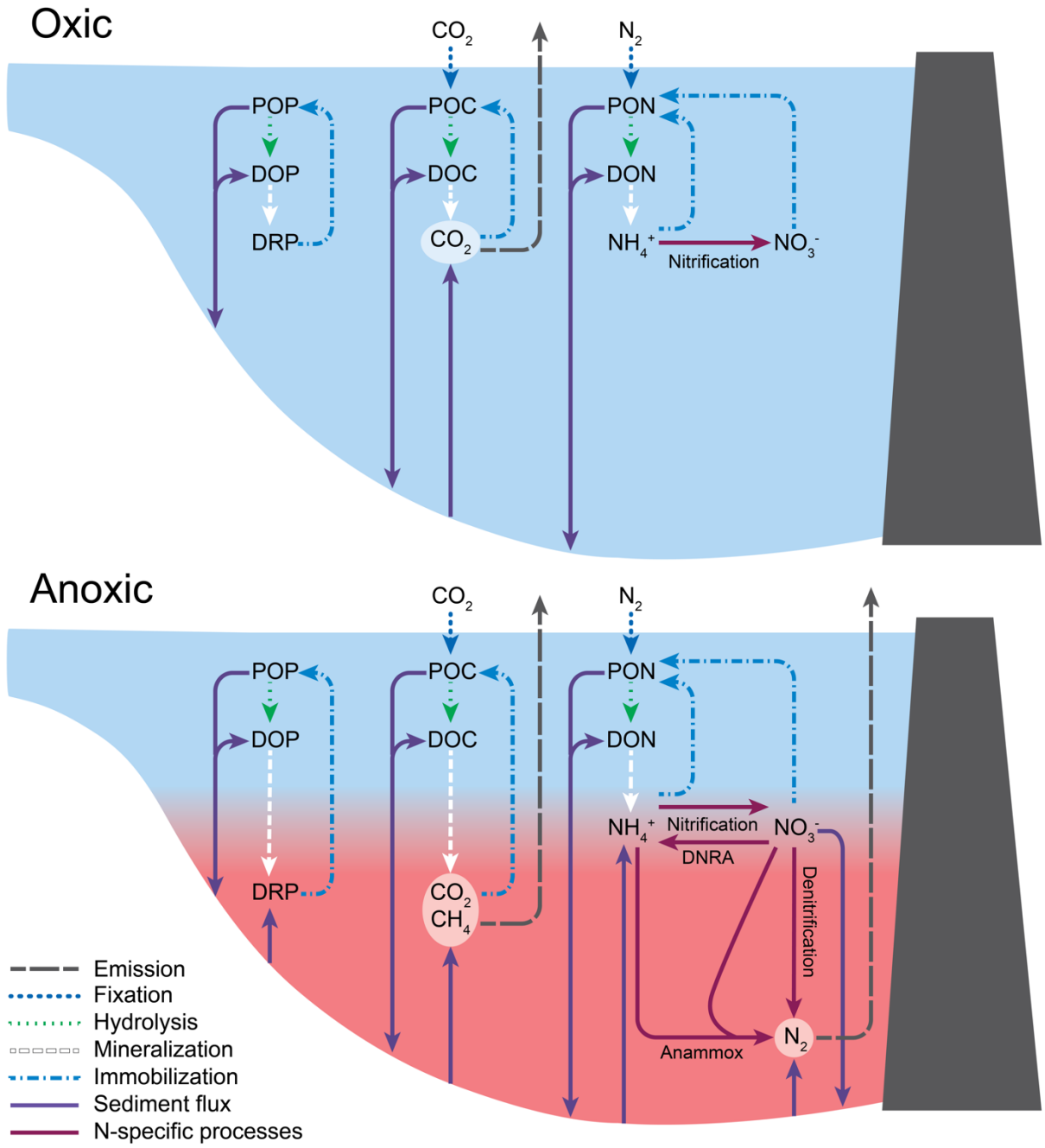

1157
1158

1159 **Fig. 2**

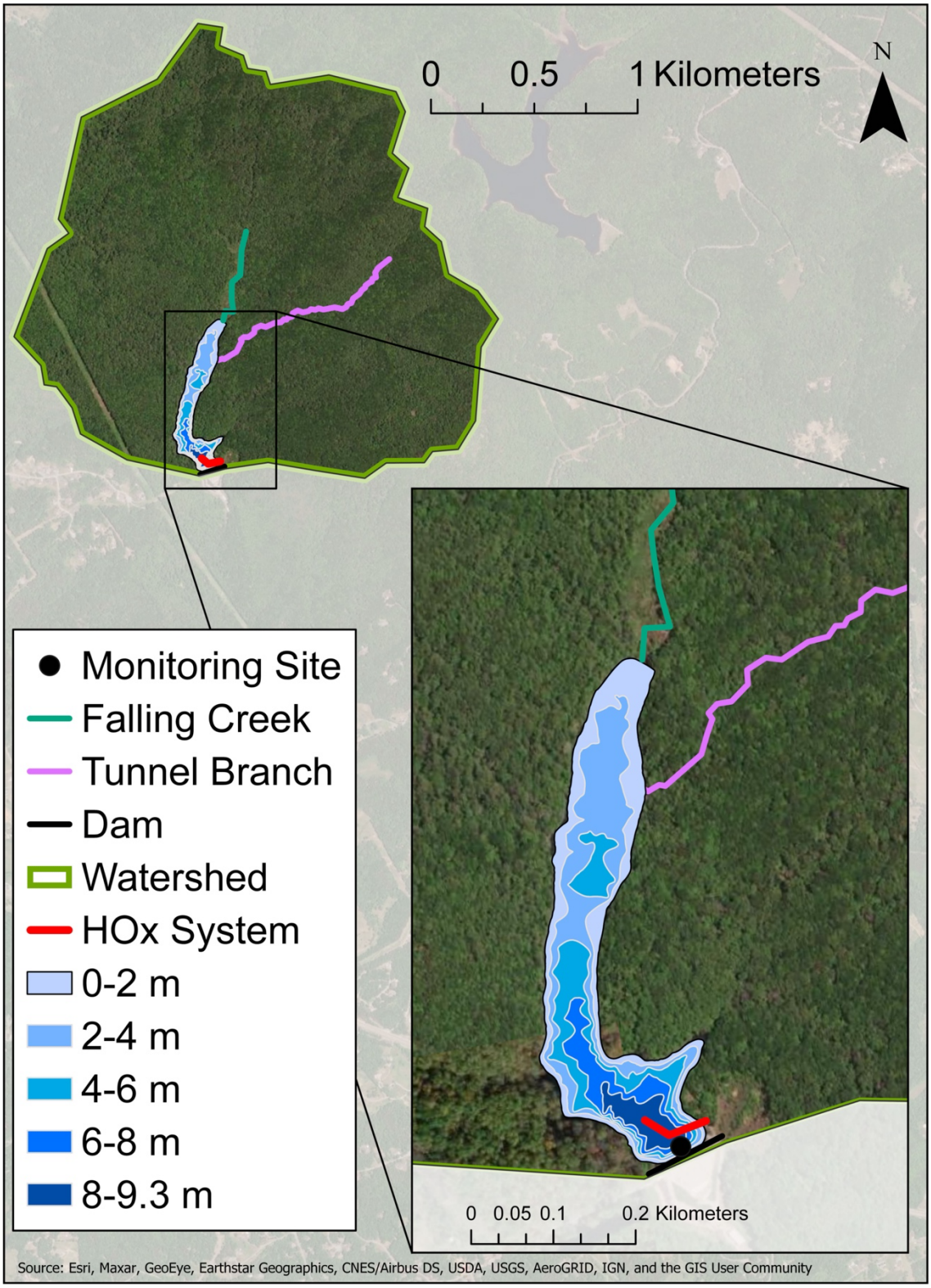

1160
1161

1162 **Fig. 3**

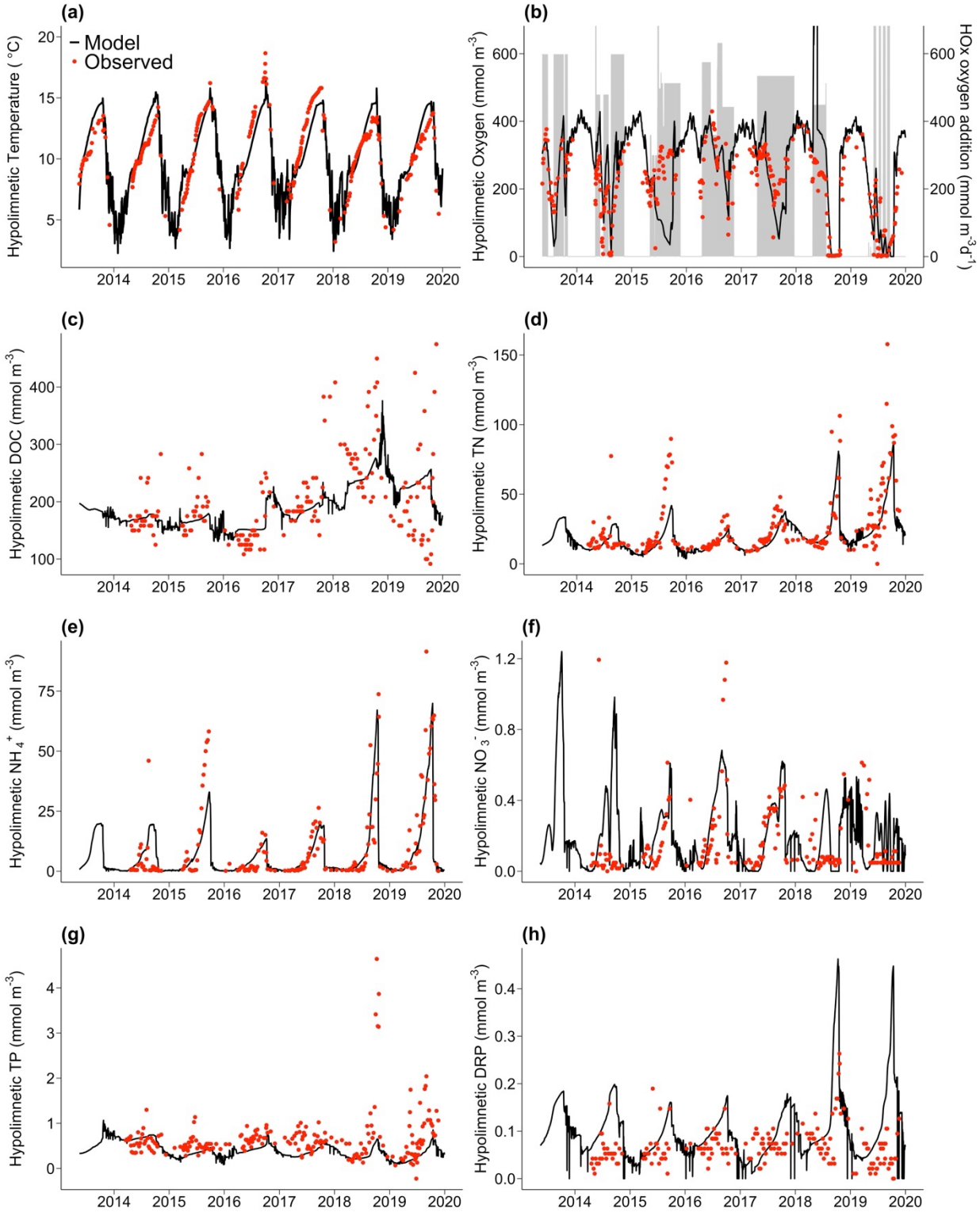

1163
1164

Fig. 4.

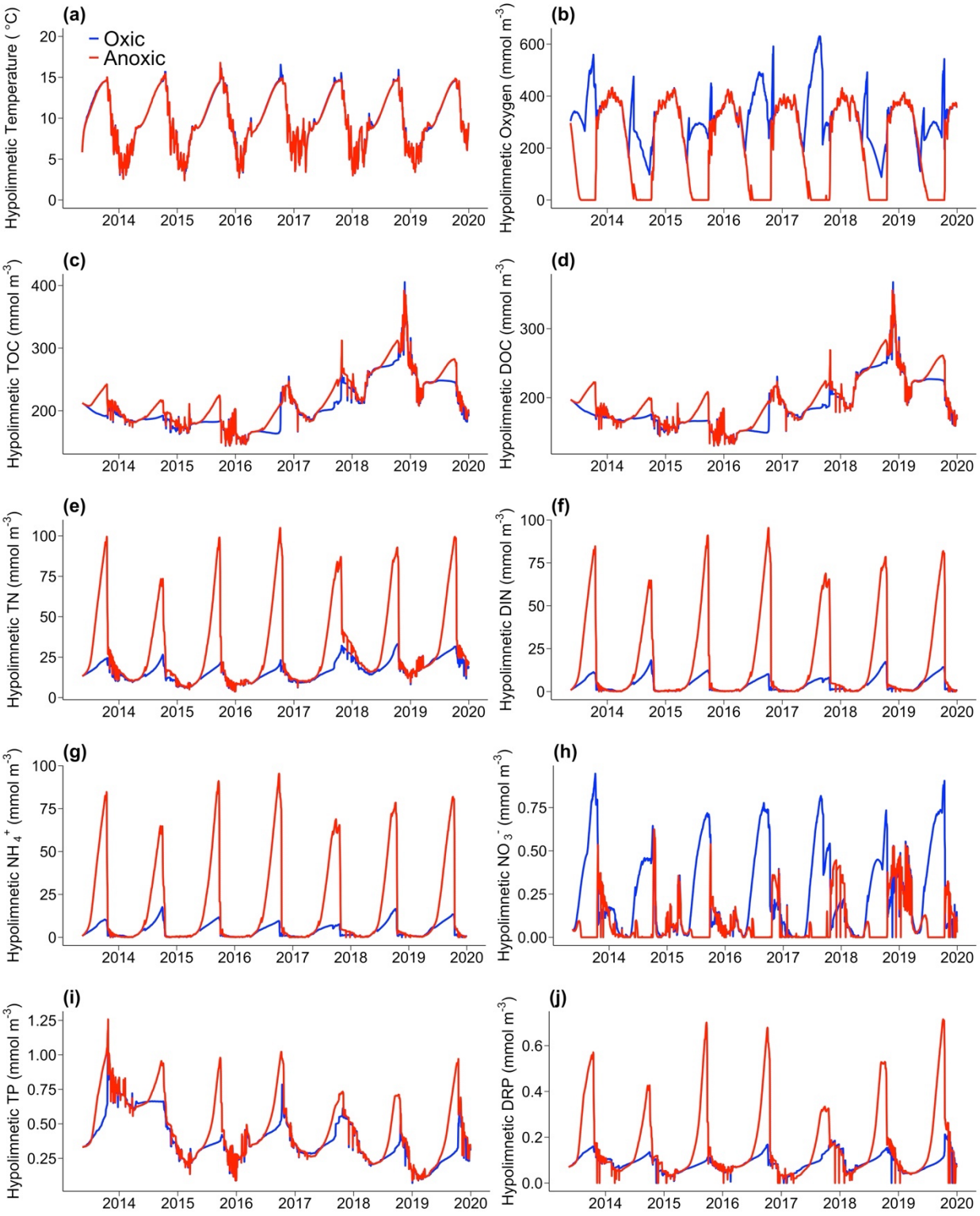
(a)
Oxic
Anoxic
Hypolimnetic Temperature (°C)
(b)
Hypolimnetic Oxygen (mmol m-3)
(c)
Hypolimnetic TOC (mmol m-3)
(d)
Hypolimnetic DOC (mmol m-3)
(e)
Hypolimnetic TN (mmol m-3)
(f)
Hypolimnetic DIN (mmol m-3)
(g)
Hypolimnetic NH4+ (mmol m-3)
(h)
Hypolimnetic NO3- (mmol m-3)
(i)
Hypolimnetic TP (mmol m-3)
(j)
Hypolimnetic DRP (mmol m-3)
2014
2015
2016
2017
2018
2019
2020

Fig. 5

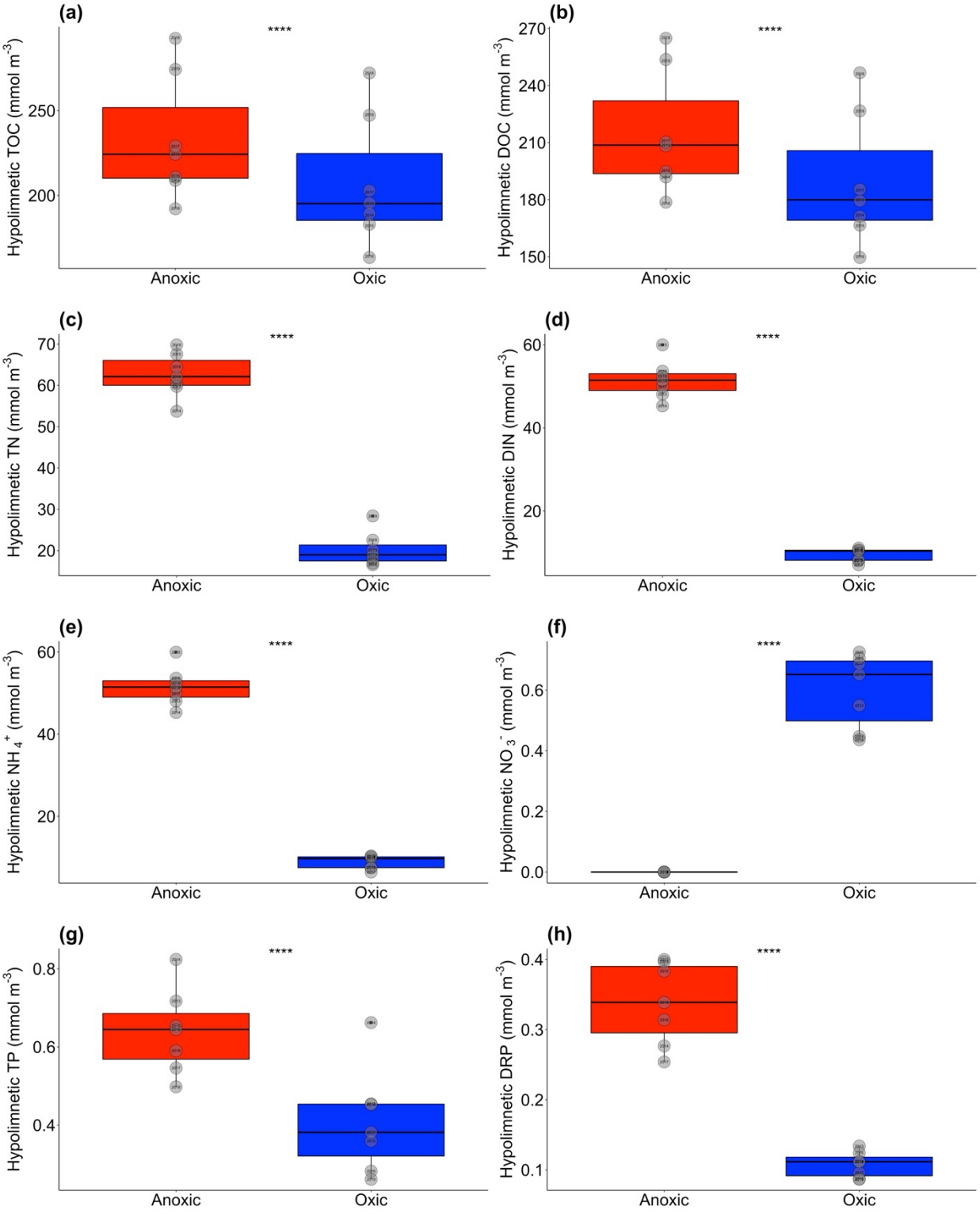
(a)
Hypolimnetic TOC (mmol m-3)
250
200
****
Anoxic
Oxic
(b)
Hypolimnetic DOC (mmol m-3)
270
240
210
180
150
****
Anoxic
Oxic
(c)
Hypolimnetic TN (mmol m-3)
70
60
50
40
30
20
****
Anoxic
Oxic
(d)
Hypolimnetic DIN (mmol m-3)
60
40
20
****
Anoxic
Oxic
(e)
Hypolimnetic NH4+ (mmol m-3)
60
40
20
****
Anoxic
Oxic
(f)
Hypolimnetic NO3- (mmol m-3)
0.6
0.4
0.2
0.0
****
Anoxic
Oxic
(g)
Hypolimnetic TP (mmol m-3)
0.8
0.6
0.4
****
Anoxic
Oxic
(h)
Hypolimnetic DRP (mmol m-3)
0.4
0.3
0.2
0.1
****
Anoxic
Oxic

Fig. 6

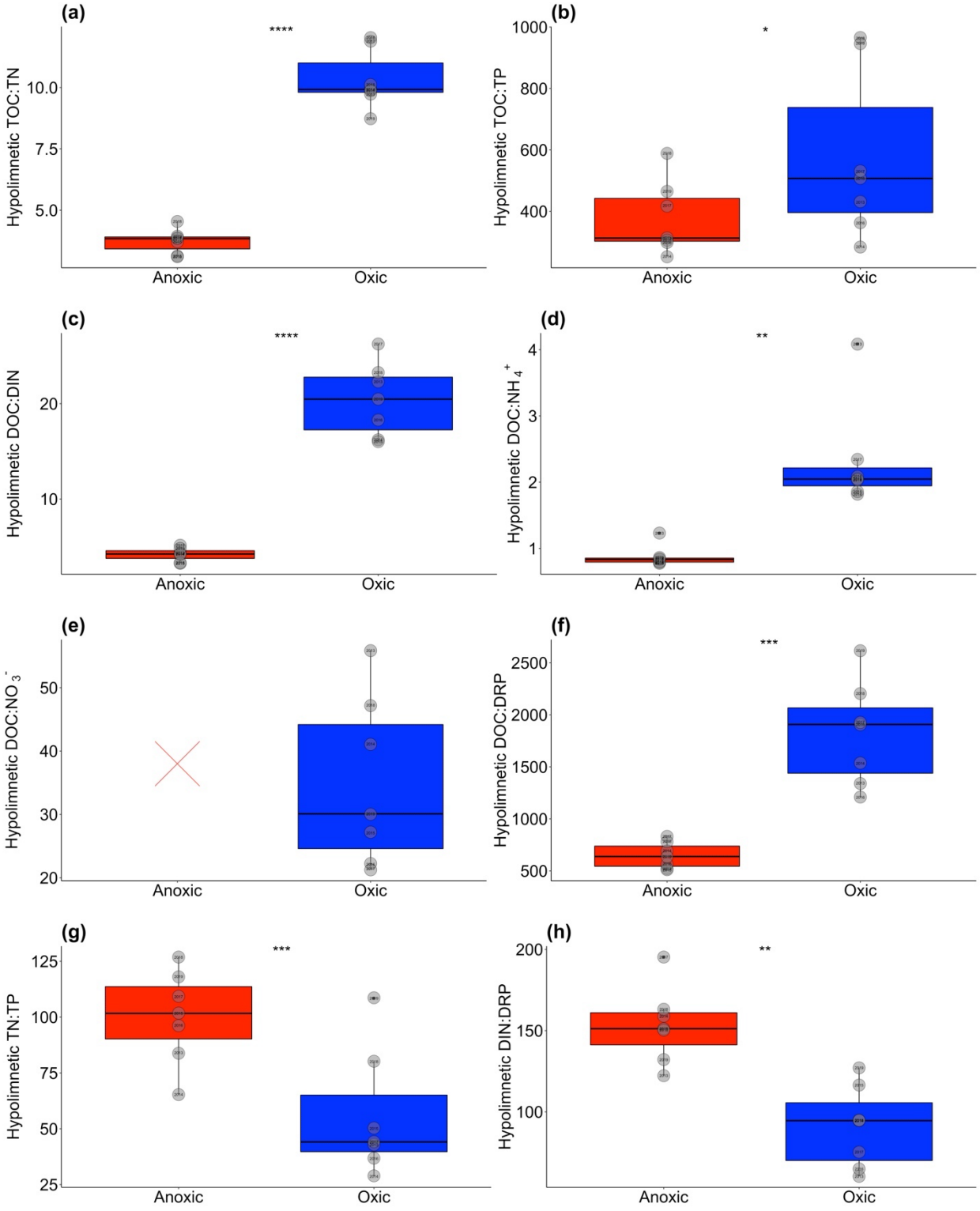
(a)
****
Hypolimnetic TOC:TN
10.0
7.5
5.0
Anoxic
Oxic
(b)
*
Hypolimnetic TOC:TP
1000
800
600
400
Anoxic
Oxic
(c)
****
Hypolimnetic DOC:DIN
20
10
Anoxic
Oxic
(d)
**
Hypolimnetic DOC:NH4+
4
3
2
1
Anoxic
Oxic
(e)
Hypolimnetic DOC:NO3-
50
40
30
20
Anoxic
Oxic
(f)
***
Hypolimnetic DOC:DRP
2500
2000
1500
1000
500
Anoxic
Oxic
(g)
***
Hypolimnetic TN:TP
125
100
75
50
25
Anoxic
Oxic
(h)
**
Hypolimnetic DIN:DRP
200
150
100
Anoxic
Oxic

1174 **Fig. 7**

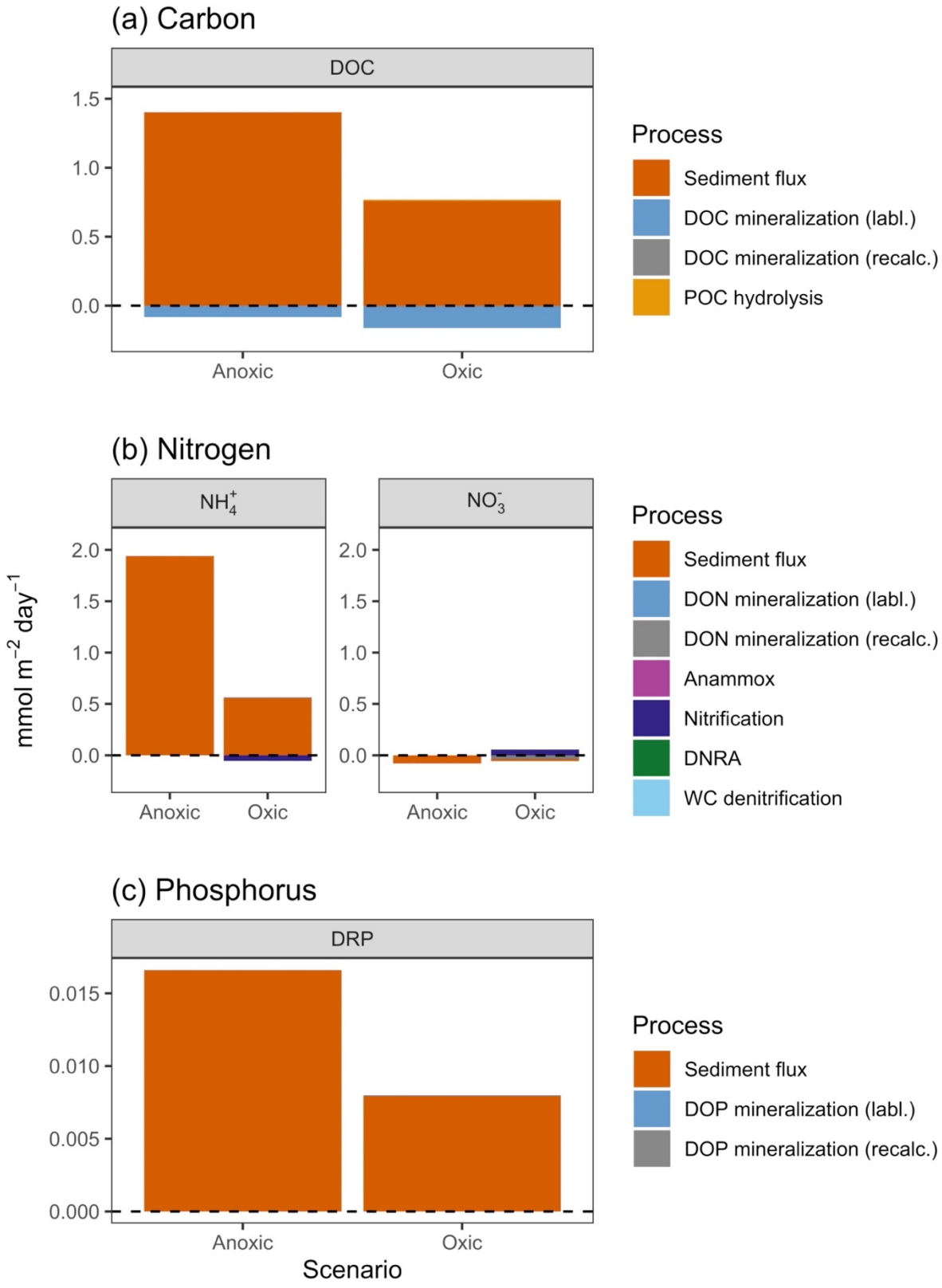

1175

Fig. 8

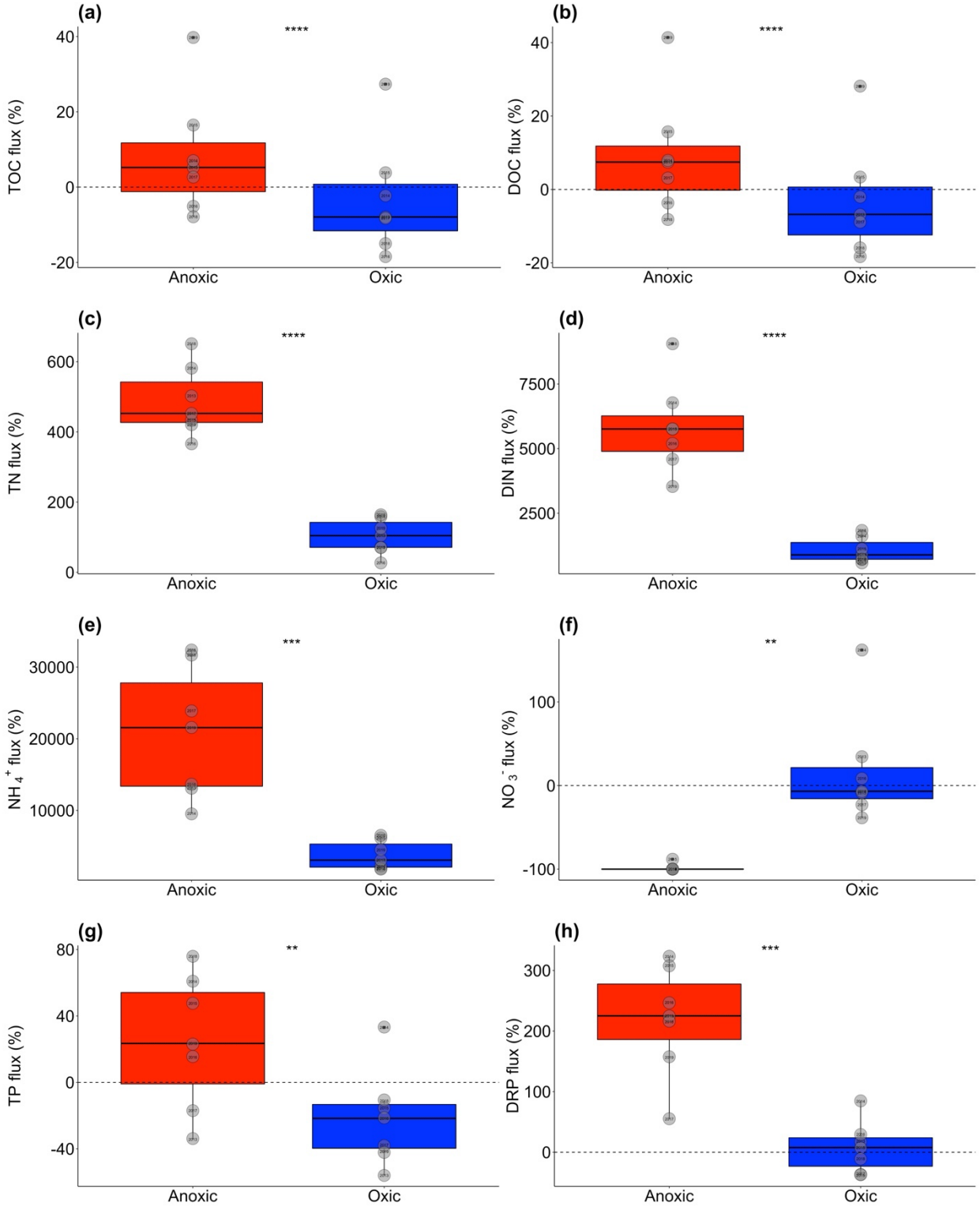
(a)
****
TOC flux (%)
40
20
0
-20
Anoxic
Oxic
(b)
****
DOC flux (%)
40
20
0
-20
Anoxic
Oxic
(c)
****
TN flux (%)
600
400
200
0
Anoxic
Oxic
(d)
****
DIN flux (%)
7500
5000
2500
Anoxic
Oxic
(e)
***
NH4+ flux (%)
30000
20000
10000
Anoxic
Oxic
(f)
**
NO3- flux (%)
100
0
-100
Anoxic
Oxic
(g)
**
TP flux (%)
80
40
0
-40
Anoxic
Oxic
(h)
***
DRP flux (%)
300
200
100
0
Anoxic
Oxic

1179 **Fig. 9**

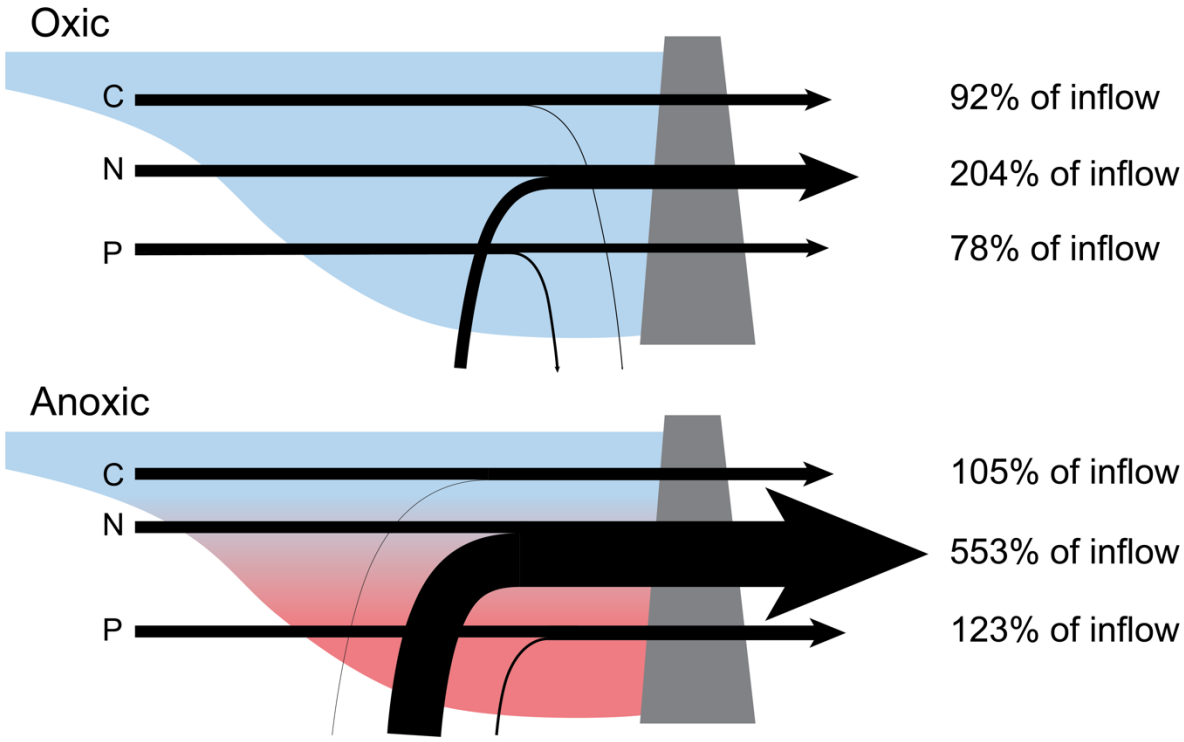

1180
1181